

Original Article

Cite this article: Saktura WM, Buckman S, Nutman AP, and Bennett VC (2021) Late Jurassic Changmar Complex from the Shyok ophiolite, NW Himalaya: a prelude to the Ladakh Arc. *Geological Magazine* **158**: 239–260. <https://doi.org/10.1017/S0016756820000400>

Received: 5 September 2019

Revised: 30 March 2020

Accepted: 10 April 2020


First published online: 10 June 2020

Keywords:

Shyok Suture Zone; Ladakh Arc; Himalaya; arc–continent collision; ophiolite; Tethys Ocean; zircon

Author for correspondence: Wanchese M. Saktura, E-mail: wms994@uowmail.edu.au

Late Jurassic Changmar Complex from the Shyok ophiolite, NW Himalaya: a prelude to the Ladakh Arc

Wanchese M. Saktura¹ , Solomon Buckman¹, Allen P. Nutman¹ and Vickie C. Bennett²

¹GeoQuEST Research Centre, School of Earth, Atmospheric and Life Sciences, University of Wollongong, Wollongong, NSW 2522, Australia and ²Research School of Earth Sciences, Australian National University, Canberra, ACT 2601, Australia

Abstract

The Shyok Suture in western Himalaya preserves a record of the opening and closure of the Mesotethys Ocean between the Shyok ophiolite and Karakoram terrane prior to the India–Eurasia collision. The formation age of the Shyok ophiolite was unknown, which impeded correlation with similar rocks along the Shyok Suture in Pakistan and corresponding sutures in Tibet. We report the first zircon U–Pb ages of a newly documented suite, here named the Changmar Complex. The Changmar Complex gabbro–granite and plagiogranite yielded SHRIMP U–Pb zircon Late Jurassic ages of 159.4 ± 0.9 Ma and 151.9 ± 1.5 Ma. Their highly positive initial ϵ_{Hf} values (+14.9 to +16.9) indicate a juvenile mantle origin, without continental crust influence on the magma source. The Shyok ophiolite represents either: (1) a separate island arc that preceded formation of the Cretaceous–Eocene Ladakh Arc; or (2) the oldest magmatism and early stage of the Ladakh Arc. Intrusive and extrusive mafic rocks from the Shyok Suture analysed in this study have typical supra-subduction zone enrichment characteristics in their geochemistry and are classified as part of the volcanic-arc ophiolite. The U–Pb age and Hf isotopic signatures for the Shyok ophiolite are similar to the Late Jurassic Matum Das tonalite within the Kohistan Arc; we therefore suggest that they are part of the same intra-oceanic island-arc system that formed in the Mesotethys Ocean prior to Late Jurassic time.

1. Introduction

The Shyok Suture extends across the Nubra region in Ladakh, northwestern India, and into northern Pakistan where it is called either the Northern or Shyok Suture (e.g. Coward *et al.* 1982; Robertson & Collins, 2002) and contains cryptic remnants of ancient oceanic crust known as the Shyok ophiolite. The Shyok Suture has received less attention than the Indus–Yarlung–Tsangpo Suture located to the south, which is thought to mark the final continent–continent collision between India and Eurasia (e.g. Searle *et al.* 1988). However, an alternative geodynamic interpretation shifts the focus of the terminal collision to the Shyok Suture, as the final step in the India–Eurasia continental collision (Khan *et al.* 2009; Burg, 2011; Bouilhol *et al.* 2013). The Shyok Suture represents an important remnant of the Mesotethys Ocean (the Bangong or Shyok Ocean) but has been an unresolved aspect of intra-Tethys geodynamics at an early stage of the development of the Himalaya. The timing of ocean closure to form the Shyok Suture has been interpreted to occur either during: (1) the Late Cretaceous Period as a result of the collision between the Kohistan–Ladakh intra-oceanic arc and Karakoram terrane of southern Eurasia (Petterson & Windley, 1985; Coward *et al.* 1987; Treloar *et al.* 1989; Rolland *et al.* 2000; Clift *et al.* 2002; Robertson & Collins, 2002; Borneman *et al.* 2015); or (2) possibly as late as the Eocene Epoch when India collided with Eurasia (Khan *et al.* 2009; Burg, 2011; Bouilhol *et al.* 2013).

A key to understanding the tectonic evolution of any plate suture is the age and nature of the intervening crust and the timing of ocean basin closure (Dewey, 2005; Stern *et al.* 2012; Draut & Clift, 2013). The identification and documentation of cryptic rock suites of intra-oceanic origin, that are often difficult to date, are critical to developing accurate tectonic reconstructions that best explain the mechanisms of ocean opening, closure and accretion of intra-oceanic terranes onto continental margins. To date, there are no geochronological data for the formation of the Shyok ophiolite that represents the basement rocks into which the Cretaceous–Eocene Ladakh Arc intrudes and overlies. Voluminous magmatic rocks of the Ladakh Arc (the Ladakh Batholith, Fig. 1) are predominantly of age 75–45 Ma (Honegger *et al.* 1982; Trivedi *et al.* 1982; Schärer *et al.* 1984; Weinberg & Dunlap, 2000; Singh *et al.* 2007; Upadhyay *et al.* 2008; Ravikant *et al.* 2009; Thanh *et al.* 2010; St-Onge *et al.* 2010; White *et al.* 2011;

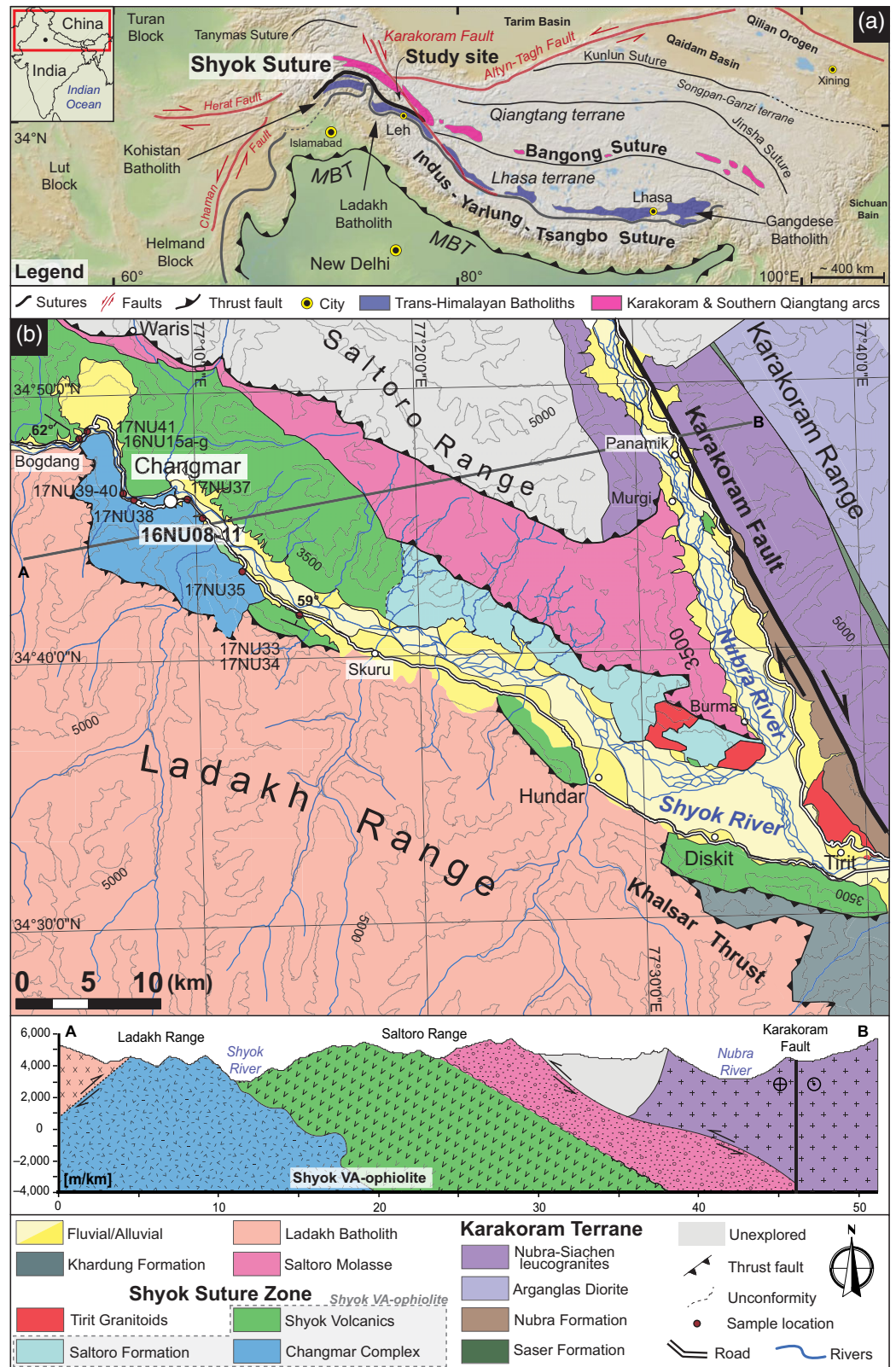


Fig. 1. (Colour online) (a) Tectonic overview of the Himalaya and Tibet showing major sutures, faults and tectonic blocks, as well as an extent of the Trans-Himalayan, Karakoram and Qiangtang plutonic rocks. Basemap sourced from GeoMapApp® software (Ryan *et al.* 2009). (b) Geological map of the Shyok and Nubra river confluence, modified after Phillips (2008) and Borneman *et al.* (2015), with addition of the Changmar Complex. Map datum: WGS84 UTM Zone 43N; elevation contour interval 500 m. The co-ordinates for each sample location are provided in Table 1.

Bouilhol *et al.* 2013; Sen & Collins, 2013; Kumar *et al.* 2017). These granitoids intrude rocks of the Shyok Suture and obscure earlier stages of the Shyok ophiolite and island-arc formation.

In this paper, we report the first Jurassic U–Pb zircon ages and Hf isotope data for newly documented gabbro-norite and

plagiogranite rock suite (here named the Changmar Complex) collected from the Shyok Suture along the Shyok Valley in NW India, near the India–Pakistan Line of Control (Fig. 1). The Jurassic rocks of the Changmar Complex are interpreted to represent the remnants of a mature island arc that developed within the Shyok ophiolite,

together referred to as the Shyok volcanic-arc ophiolite (VA-ophiolite). New data presented here are compared with rocks of similar age and composition reported from the Kohistan, Karakoram and Tibet regions, to evaluate the feasibility of a divergent double subduction zone as a potential mechanism for the closure of the Shyok and Bangong sutures.

2. Geological background

The geological elements involved in the tectonic collision along the Shyok and Bangong sutures, from north to south, are: (1) the active continental margin of Eurasia, composed of the Karakoram and Southern Qiangtang terranes (Fig. 2; e.g. Searle *et al.* 1990; Ravikant *et al.* 2009; Groppo *et al.* 2019); (2) the Mesotethys Ocean, represented by ophiolites, ophiolitic mélanges and intra-oceanic arc system (the Shyok VA-ophiolite and Kohistan Arc) along the Shyok Suture in the western Himalaya (e.g. Rolland *et al.* 2000; Cliff *et al.* 2002; Robertson & Collins, 2002; Thanh *et al.* 2012; Borneman *et al.* 2015), and a series of ophiolites and ophiolitic mélanges along the Bangong Suture in Tibet (e.g. Baxter *et al.* 2009; Fan *et al.* 2015b); and (3) the Lhasa microcontinent (e.g. Zhu *et al.* 2011, 2013). The terranes involved in the collision along the Shyok–Bangong Suture are summarized on the tectonostratigraphic columns on Figure 2, and major terranes are discussed below.

2.a. Karakoram Arc

An Andean-type convergent-margin magmatism occurred along the southern Eurasian continent throughout Jurassic–Cretaceous time, giving rise to the Karakoram Arc (e.g. Rex *et al.* 1988; Groppo *et al.* 2019). The preserved part of this continental arc is c. 700 km long and 30 km wide, and consists of an intermediate to felsic calc-alkaline plutonic complex in the northwestern Himalaya (e.g. Searle & Hacker, 2018) that intrudes the Palaeozoic–Mesozoic sedimentary rocks of the Karakoram terrane (Gaetani, 1997). The Karakoram Arc was active from Late Jurassic – Late Cretaceous time (162–83 Ma, see Fig. 2; Borneman *et al.* 2015; Groppo *et al.* 2019; Pundir *et al.* 2020) as the oceanic slab of the Mesotethys was subducting to the north beneath Eurasia, until the Kohistan Arc and Shyok VA-ophiolite collided with Eurasia and shut off slab-driven magmatism (e.g. Borneman *et al.* 2015; Groppo *et al.* 2019). The intrusive rocks of the Karakoram Arc are characterized by negative ε_{Hf} values of -4 to -2 (Ravikant *et al.* 2009), reflecting the assimilation of old and evolved continental crust (e.g. Amelin *et al.* 1999). Calc-alkaline rocks younger than c. 83 Ma have not been documented within the Karakoram Block, but intrusions of the extensive post-collisional Nubra–Siachen leucogranites (Fig. 1) occurred between 21 and 13 Ma (e.g. Searle & Hacker, 2018).

2.b. Tethyan oceans

In the Tethyan realm the Palaeotethys and Neotethys oceans are well-defined geographically with well-established tectonic relationships with their bounding terranes (e.g. Şengör, 1984; Dilek & Furnes, 2019), but this is not so clear for the Mesotethys Ocean. The Palaeotethys and Neotethys oceans were associated with the beginning of the Tethyan realm (Palaeotethys) during Early Devonian time and its demise (Neotethys) in the Palaeogene Period (Searle *et al.* 1987; Aitchison *et al.* 2011; Metcalfe, 2013). In the Tethyan tectonic framework, the Mesotethys

Ocean existed at the transition between the Palaeotethys and the Neotethys (Permian? – Late Cretaceous; Metcalfe, 2013). The Mesotethys is regarded as having formed during the rift and drift of the Cimmerian continent from Gondwana during Late Palaeozoic – Mesozoic time (e.g. Metcalfe, 1996). Northwards drift of the Cimmerian continent consumed the Palaeotethys in the north, while opening the Mesotethys to the south (Metcalfe, 1996, 2013). Closure of the main Palaeotethys Ocean basin occurred from the west in the Pamirs to the east in the Malay Peninsula along the following sutures: Jinsha (Tanymas), Changning–Menglian, Chiang Mai/Inthanon, Chanthaburi and Bentong–Raub (Metcalfe, 2013; Zanchetta *et al.* 2018).

The Mesotethys Ocean has also been called the Bangong–Nujiang Tethyan Ocean (e.g. Zhu *et al.* 2013), the Bangong Ocean (Pullen *et al.* 2011) or the Shyok Ocean/Sea/Basin (Searle *et al.* 1999; Thanh *et al.* 2012; Chapman *et al.* 2018), and its oceanic crust referred to as the Kshiroda Plate (Jagoutz *et al.* 2015). Two mechanisms were proposed for the closure of the Mesotethys: (1) northwards subduction beneath Eurasia (e.g. Allègre *et al.* 1984); and (2) northwards subduction beneath Eurasia and concurrent southwards subduction beneath Gondwana (Metcalfe, 2013; Zhu *et al.* 2013, 2016), that led to rifting of the micro-continental Lhasa terrane from northern Gondwana during the Late Triassic – Early Jurassic period (e.g. Zhu *et al.* 2011). To the north, the Mesotethys Ocean was bound from west to east by the Karakoram terrane, the Southern Qiangtang and the Sibumasu terrane (Metcalfe, 2013; Groppo *et al.* 2019). To the south, the Mesotethys was bound by the intra-oceanic Kohistan–Shyok island-arc system, which was located to the west of the micro-continental ribbon of the Lhasa terrane (e.g. Groppo *et al.* 2019). The Eurasian margin and southern Mesotethys terranes are now separated by the Shyok Suture in Pakistan (e.g. Petterson & Treloar, 2004) and Ladakh (e.g. Borneman *et al.* 2015) and the Bangong Suture in Tibet (e.g. Baxter *et al.* 2009) and possibly the Myitkyina Suture and Shan Boundary in SE Asia (Liu *et al.* 2016). Ophiolitic and island complexes along these sutures mark the extant Mesotethys Ocean (Baxter *et al.* 2009; Liu *et al.* 2016).

Rifting of the Lhasa terrane from Gondwana during Late Triassic – Early Jurassic time opened the Neotethys Ocean (Zhu *et al.* 2011). This ocean basin was further separated from the Mesotethys by the initiation of the Kohistan–Shyok intra-oceanic arc system during Late Jurassic time (Jagoutz *et al.* 2015, 2018). The closure of the Neotethys Ocean along the Indus–Yarlung–Tsangpo Suture marks the final stage of the Himalayan orogeny, and has been extensively covered in the literature (e.g. Searle *et al.* 1987; Gibbons *et al.* 2015; Aitchison *et al.* 2007; Searle & Treloar, 2019). The Indus–Yarlung–Tsangpo Suture marks the boundary between Eurasia and India in Ladakh, and Lhasa and India in Tibet, with intra-oceanic-arc terranes and ophiolites of the Neotethys preserved along the suture (Aitchison *et al.* 2007; Hébert *et al.* 2012; Metcalfe, 2013; Buckman *et al.* 2018; Walsh *et al.* 2019).

2.c. Tethyan intra-oceanic-arc system

There is an ongoing debate over whether the Tethyan intra-oceanic arc that consists of the Kohistan Arc and Shyok VA-ophiolite first collided with Eurasia or India. In the first hypothesis, the arc accreted to Eurasia between c. 85 and 75 Ma along the Shyok Suture and the final continent–continent collision between India and Eurasia took place later along the Indus–Yarlung–Tsangpo Suture (Petterson & Windley, 1985; Treloar *et al.* 1989; Robertson

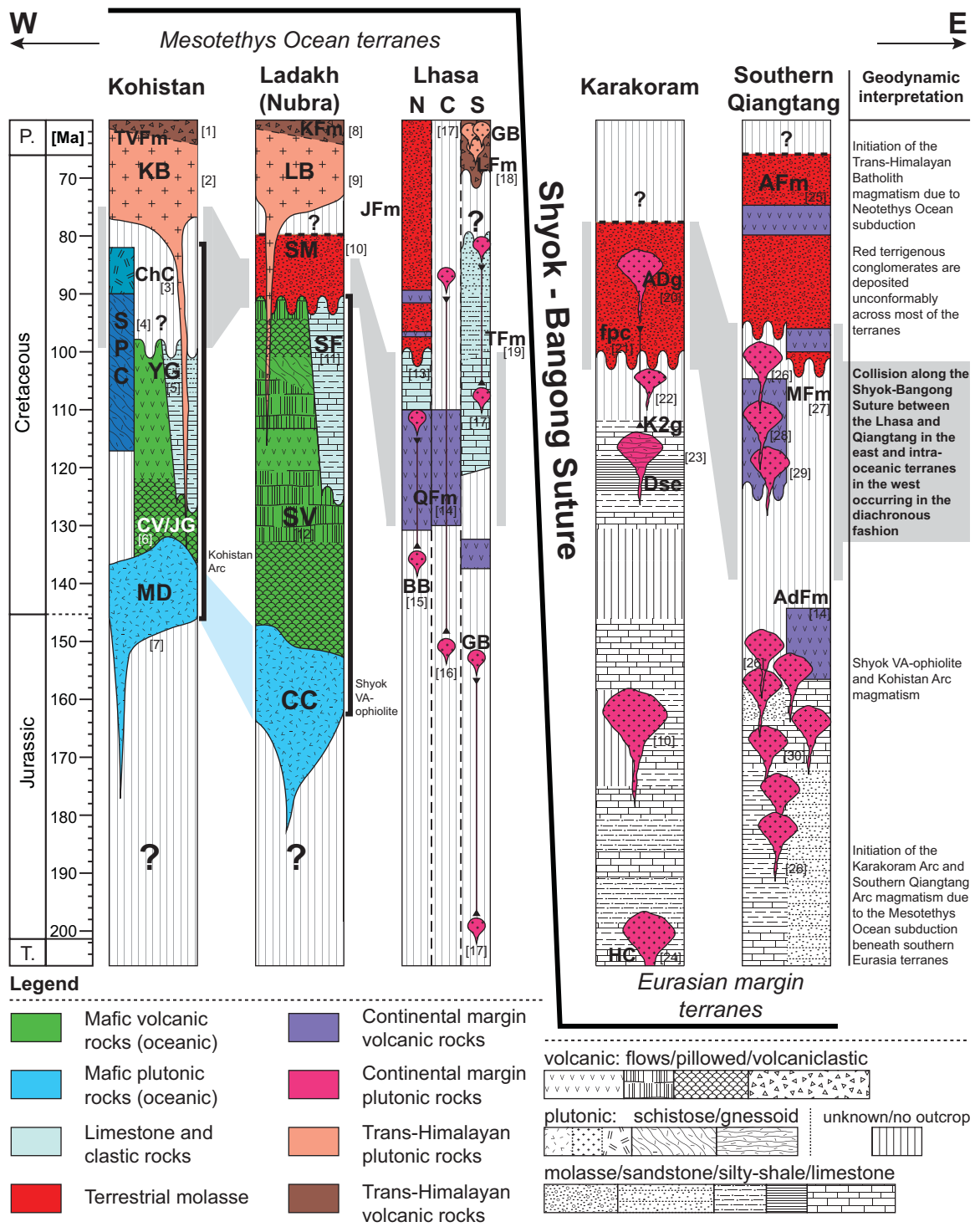


Fig. 2. (Colour online) Generalized tectonostratigraphic columns for the regions discussed. The depicted sedimentary sequences for the Karakoram terrane shown without colour represent country rocks and do not correspond to the geological timescale. Stratigraphic columns are shown from west (left) to east (right). The along-strike (E–W) variation in rock types is also captured within each column for the Lhasa, Karakoram and Southern Qiangtang terranes and follows the same west (left) to east (right) direction. AdFm – Amdo Formation; ADg – Aguil Dara granodiorite; AFm – Abushan Formation; BB – Baingoin Batholith; C – Central Lhasa; CC – Changmar Complex; ChC – Chilas Complex; CV/JG – Chalt Volcanics and Jalgot Group; Dse – Doksam sequence; fpc – fluvial polygenic conglomerate; GB – Gangdese Batholith; HC – Hushe Complex; JFm – Jingzhushan Formation; K2g – K2 gneiss; KB – Kohistan Batholith; KFM – Khardung Formation; LB – Ladakh Batholith; LFM – Linzizong Formation; MD – Matum Das tonalite and equivalent Jurassic plutonic rocks; MFm – Meirigicuo Formation; N – North Lhasa; QFm – Qushenla Formation; S – Southern Lhasa; SF – Saltoro Formation; SM – Saltoro Molasse; SV – Shyok Volcanics; TFm – Tadena Formation; TVFm – Teru Volcanic Formation (Shamran Volcanics); YG – Yasin Group. Sources of the geological and geochronological data: [1] Khan et al. (2004); [2] Bouilhol et al. (2013); [3] Schaltegger et al. (2002); [4] Dhuime et al. (2007); [5] Pudsey (1986); [6] Khan et al. (2007); [7] Jagoutz et al. (2018); [8] Dunlap & Wysoczanski (2002); [9] Honegger et al. (1982); [10] Borneman et al. (2015); [11] Juyal (2006); Upadhyay (2014); [12] Rolland et al. (2000); Dunlap & Wysoczanski (2002); Thanh et al. (2012); [13] Wang et al. (2013); [14] Zhu et al. (2016); [15] Haider et al. (2013); [16] Zhu et al. (2011); [17] Ji et al. (2009); [18] Zhou et al. (2004); [19] Leier et al. (2007); [20] Groppo et al. (2019); [21] Gaetani (2016); [22] Ravikant et al. (2009); Thanh et al. (2010); Kumar et al. (2017); Pundir et al. (2020); [23] Searle et al. (1990); [24] Rex et al. (1988); [25] Li et al. (2013); [26] Li et al. (2017b); [27] Fan et al. (2015a); [28] Li et al. (2017a); [29] Li et al. (2017c); [30] Li et al. (2014).

& Degnan, 1994; Clift *et al.* 2002; Robertson & Collins, 2002; Borneman *et al.* 2015). In the second hypothesis, the arc collided first with India at *c.* 50 Ma and the final continental collision occurred at *c.* 40 Ma along the Shyok Suture (Khan *et al.* 2009; Burg, 2011; Bouilhol *et al.* 2013). Both models have merit; however, more data on the early development stages of the magmatic arcs within the Tethyan realm are needed to understand geodynamic evolution of this intra-oceanic system.

2.c.1. Shyok VA-ophiolite

The Shyok VA-ophiolite within the Shyok Suture is a relic of an ocean basin and is strongly dismembered in comparison to the other Tethyan ophiolites such as the Spongtag (Pedersen *et al.* 2001; Buckman *et al.* 2018) or Semail (Coleman, 1981; Searle & Cox, 1999). VA-ophiolitic rocks crop out along the NW–SE-trending Shyok Suture of the Shyok Valley and were described as ‘Ophiolitic Mélange’ (Gansser, 1974; Frank *et al.* 1977). These rocks are tectonically dismembered, but are not enveloped in schistose mud or serpentinite matrix as observed in the Northern Suture, Pakistan (e.g. Pudsey, 1986). This suggests the Shyok VA-ophiolite was emplaced via obduction rather than in the form of a diapiric mélange. Pervasive deformation of the rock units has resulted in poor preservation of the original ophiolitic stratigraphy and outcrops of the Shyok VA-ophiolite occur as a disrupted ophiolitic sequence (e.g. Dunlap & Wysoczanski, 2002; Thanh *et al.* 2012).

The most abundant ophiolitic element present within the Shyok Suture are the Shyok Volcanics (Fig. 1), which along with the Changmar Complex compose the Shyok VA-ophiolite. The Shyok Volcanics display pillow basalt structures with minor carbonate lenses (Fig. 3b,c). This formation has been deformed and metamorphosed to greenschist facies (Dunlap & Wysoczanski, 2002; Thanh *et al.* 2012). There is an ambiguity in nomenclature for the mafic volcanic rocks that are distributed along the Shyok River (Fig. 1). These are commonly referred to as the Shyok Volcanics by Frank *et al.* (1977), Sharma *et al.* (1978), Rai (1983), Bhutani *et al.* (2009) and Borneman *et al.* (2015) or the Shyok Formation by Thakur *et al.* (1981), Weinberg *et al.* (1999) and Dunlap & Wysoczanski (2002). However, these rocks were also called the Shyok volcanite by Upadhyay *et al.* (1999), mélange unit by Rolland *et al.* (2000), metavolcanics by Thanh *et al.* (2012) or the Shyok Volcanic Formation by Ravikant *et al.* (2009). The originally named Shyok Volcanics most frequently refer to the greenschist mafic volcanic rocks that include pillow basalts with minor chert or limestone that are interpreted to be the volcanic portion of an ophiolite sequence. They form part of the Saltoro Range and crop out near Diskit and along the length of the Shyok Valley in the northern Nubra region up to Bogdang village (Fig. 1; Frank *et al.* 1977; Thakur *et al.* 1981; Thanh *et al.* 2012). However, the name Shyok Formation is used for a greenschist facies rocks that are predominantly sedimentary and occur in the southern Nubra region, and consist of marbles, slates, andesites and andesitic volcanoclastic rocks (Dunlap & Wysoczanski, 2002; Ehiro *et al.* 2007; Kumar *et al.* 2016). The Shyok Formation possibly overlies the basaltic volcanic pile of the Shyok Volcanics (Shyok VA-ophiolite), representing a stratigraphical continuation; however, field relationships have not been established.

Rolland *et al.* (2000) suggested that the Shyok Volcanics are of middle Cretaceous age (108–92 Ma) based on the presence of *Orbitolina* foraminifera in limestones interbedded with the volcanic rocks. This supports the interpretation that the Shyok

Volcanics are related to the Shyok Formation, which also contains *Orbitolina* fossils. The *Orbitolina* fossils in the Shyok Formation were found in the Changthang area near the village of Tsoltak, *c.* 90 km SE from the area on Figure 1, and were dated as of early–middle Albian age (Reuber, 1990; Matsumaru *et al.* 2006). This age conflicts with the fossil ages of Rolland *et al.* (2000); however, the exact stratigraphic relationships between these formations are unknown.

The Saltoro Formation (Fig. 1) consists of siltstones, turbidite sandstones, slates, phyllites, shallow-water limestones and marbles containing Aptian–Albian *Horiopleura*, *Orbitolina*, Radiolitidae and Rudist fossils (Upadhyay, 2001, 2014; Juyal, 2006), as well as Cheilostomata bryozoans of possible Jurassic age (Upadhyay *et al.* 1999). The Saltoro Formation unconformably overlies the Shyok Volcanics (Upadhyay, 2001, 2014; Juyal, 2006), and the formations are similar in age, which suggests that the Saltoro Formation likely represents a sedimentary cover of the Shyok VA-ophiolite. There is no direct contact between the Saltoro Formation and the Shyok Formation from the southern Nubra region, but there is an overlap in Aptian–Albian age between these two formations. Based on the composition of each formation, it is possible that the Saltoro and Shyok formations formed the uppermost sedimentary section of the Shyok VA-ophiolite, where the Shyok Formation was deposited close to the volcanic centre and the Saltoro Formation away from it. Upadhyay (2014) noted similarities between Rudist fauna and microfaunal assemblages of the Saltoro Formation and those of the Yasin Group in northern Kohistan, which unconformably overlies volcanic rocks of the Kohistan Arc (e.g. Bard, 1983; Fig. 2), just as the Saltoro Formation unconformably overlies the Shyok Volcanics of the Shyok VA-ophiolite. The broad range in the biostratigraphic ages from the Saltoro Formation suggests that the Shyok VA-ophiolite obduction did not occur until after early–middle Cretaceous time.

Due to the lack of a well-defined plateau in an ^{40}Ar – ^{39}Ar age, the radiometric dating of the Shyok Volcanics resulted in only a minimum formation age of *c.* 125 Ma (Dunlap & Wysoczanski, 2002; Borneman *et al.* 2015). Thanh *et al.* (2012) used the K–Ar method to date metamorphic albite in boninite and obtained an age of 104.4 ± 5.6 Ma for the metamorphism of the Shyok Volcanics, which they interpreted as a minimum age for the exhumation of the ophiolitic rocks. The crystallization age for these rocks is yet to be established, but must be older than the middle Cretaceous metamorphic ages.

Red conglomerates and sandstones of the Saltoro Molasse unconformably overlay the Shyok Volcanics and Saltoro Formation (Fig. 2; Upadhyay *et al.* 1999). The Saltoro Molasse was interpreted as deposited in a syn- to post-collisional environment, on top of the Shyok Suture rocks; it therefore post-dates the collision along the Shyok Suture (Upadhyay *et al.* 1999; Borneman *et al.* 2015). The youngest detrital zircon age population of *c.* 92 Ma from this molasse indicates when the collision between the Shyok VA-ophiolite and Karakoram terrane was completed (Borneman *et al.* 2015). A granitic dyke with an age of *c.* 85 Ma intrudes the unconformity between the Saltoro Molasse and Shyok Volcanics, and provides another control on the depositional age of this molasse (92–85 Ma; Borneman *et al.* 2015).

2.c.2. Field relationship similarities along the Shyok Suture

The Shyok Volcanics in the Ladakh region could be related to the Chalt Volcanics in Kohistan as suggested by Thanh *et al.* (2012); this is based on their basic composition, presence of boninites and



Fig. 3. (Colour online) (a) Gabbronorite (16NU08) and plagiogranite (16NU09) exposure from the Changmar Complex along the Diskit–Turtuk highway; (b) exposure of the pillow basalts of the Shyok Volcanics (16NU15) in the northwestern part of the Shyok Valley (34.80667° N, 77.07969° E); (c) carbonate lenses (outlined) within the Shyok Volcanics (34.80667° N, 77.07969° E); (d) close-up of a foliated granodiorite of the Ladakh Batholith which contains abundant mafic xenoliths from the Shyok Volcanics and is intruded by pre- and post-deformation dykes (34.822086° N, 76.928657° E); (e) outcrop where close-up (d) was taken, showing more xenoliths.

Table 1. Whole-rock major and trace element geochemistry for the Changmar Complex and Shyok Volcanics from this study with the corresponding sample locations (WGS84 UTM Zone 43N). B – basalt; BT – basaltic trachyandesite; G – gabbronorite; H – harzburgite; Lat. – latitude; Long. – longitude; N – norite; P – plagiogranite; PB – pillow basalt; TB – trachybasalt.

	Changmar Complex								Shyok Volcanics											
	16NU08	16NU09	16NU10	16NU11	17NU38	17NU39	17NU40	17NU35	16NU15a	16NU15b	16NU15c	16NU15d	16NU15e	16NU15f	16NU15g	17NU33	17NU34	17NU36	17NU37	17NU41
Rock type	G	P	P	G	P	P	N	H	TB	TB	B	BT	PB	TB	PB	BT	B	BT	B	B
Lat. (°)	34.75556	34.75558	34.75558	34.75558	34.76776	34.77157	34.77202	34.72167	34.80631	34.80637	34.80643	34.80651	34.80660	34.80678	34.80668	34.69437	34.69381	34.76711	34.76753	34.81123
Long. (°)	77.17168	77.17168	77.17164	77.17164	77.12009	77.11198	77.11217	77.20082	77.07962	77.07964	77.07965	77.07967	77.07968	77.07974	77.07969	77.24322	77.24317	77.16116	77.16041	77.08590
SiO ₂	50.41	52.18	57.93	46.45	50.03	57.55	55.06	37.48	49.96	49.04	48.96	49.91	38.72	49.25	44.89	50.84	48.82	52.83	43.48	50.54
TiO ₂	0.81	0.39	0.65	1.35	0.49	0.58	0.60	0.05	1.82	1.80	1.03	2.12	0.75	2.15	0.97	0.74	0.61	1.11	0.42	1.18
Al ₂ O ₃	19.05	24.58	16.11	11.03	22.69	16.84	17.94	6.06	14.87	14.39	14.51	14.99	10.91	15.82	12.89	16.52	16.77	16.02	8.63	12.91
Fe ₂ O ₃	11.02	4.58	8.33	19.10	6.67	6.95	7.60	12.51	11.89	13.31	10.65	13.21	8.31	13.38	11.33	12.30	7.47	9.47	11.20	14.00
MnO	0.19	0.07	0.15	0.29	0.12	0.13	0.13	0.18	0.17	0.19	0.15	0.18	0.15	0.16	0.17	0.18	0.12	0.15	0.22	0.22
MgO	4.45	1.37	3.11	7.89	1.84	2.83	2.80	29.04	6.04	5.83	9.51	4.66	5.81	5.78	12.37	6.98	6.59	6.12	19.61	6.73
CaO	10.96	9.69	6.43	9.80	9.33	3.79	6.47	3.90	7.71	7.19	7.61	6.74	18.93	5.43	12.34	2.62	11.08	6.58	10.32	9.51
Na ₂ O	2.75	4.58	2.43	1.01	3.78	3.40	2.72	0.14	4.57	4.64	3.77	5.36	2.63	4.41	0.64	5.22	3.25	5.52	0.49	3.05
K ₂ O	1.24	1.43	3.62	1.39	1.85	3.77	3.13	0.01	0.60	0.71	0.18	0.56	1.66	1.13	0.66	0.61	0.05	0.13	0.25	0.07
P ₂ O ₅	0.34	0.32	0.22	0.27	0.42	0.19	0.20	< 0.01	0.23	0.29	0.10	0.38	0.12	0.39	0.10	0.07	0.08	0.19	0.10	0.08
SO ₃	0.02	0.02	< 0.01	0.01	0.03	0.01	0.02	0.65	0.10	0.03	0.01	0.13	0.01	0.18	0.03	0.01	0.29	0.03	0.00	0.04
LOI	0.25	1.19	1.08	1.72	2.07	2.70	1.99	8.99	2.15	2.63	3.31	2.38	12.63	2.70	4.35	3.52	4.01	1.68	5.80	1.38
Total	101.49	100.40	100.06	100.31	99.32	98.73	98.68	99.01	100.10	100.05	99.78	100.61	100.64	100.78	100.74	99.61	99.14	99.81	100.52	99.71
Trace elements (ppm)																				
Ag	0.12	0.11	0.08	0.12	0.25	0.04	0.14	0.07	0.06	0.08	0.08	0.07	0.04	0.07	0.05	0.03	0.02	0.1	0.05	0.16
As	1.70	3.00	4.20	2.00	3.2	3.2	2.7	13.4	1.40	1.30	1.20	6.10	0.30	4.10	1.40	1.2	3.3	1.3	1.5	1.2
Ba	190.00	220.00	320.00	180.00	180	270	220	<10	120.00	140.00	30.00	100.00	150.00	150.00	160.00	80	20	60	40	10
Be	0.59	0.62	0.89	0.45	0.54	0.63	0.71	<0.05	0.54	0.53	0.31	0.72	0.14	0.55	0.36	0.25	0.19	0.37	0.48	0.39
Bi	0.03	0.04	0.12	0.03	0.04	0.06	0.06	0.01	0.01	0.01	<0.01	0.01	<0.01	0.02	0.01	0.01	0.01	0.01	0.01	0.01
Cd	0.08	0.06	0.08	0.15	0.05	0.03	0.06	0.04	0.04	0.05	0.10	0.06	0.08	0.06	0.14	0.06	0.08	0.1	0.06	0.09
Ce	30.30	15.20	52.90	33.50	32.8	53	38.1	0.55	21.90	25.10	8.30	28.40	7.11	32.80	8.09	11.4	8.33	26.5	18.75	8.62
Cr	54.00	39.00	59.00	47.00	5	8	9	879	96.00	45.00	52.00	39.00	555.00	60.00	602.00	8	81	65	1660	40
Cs	2.32	1.16	7.70	4.84	2.33	2.93	2.69	0.41	0.88	1.16	0.37	1.84	2.00	2.01	0.82	1.05	0.54	0.26	1.61	0.23
Cu	213.00	237.00	175.00	257.00	85.1	64.1	110.5	4	39.50	52.80	128.00	30.40	66.90	37.00	38.30	124.5	81.6	132	137	123.5
Ga	18.55	20.20	16.45	14.75	18.45	13	17.45	3.87	16.70	16.30	12.85	19.05	9.93	16.75	16.60	20.2	13.15	14.3	10.65	16.3
Ge	0.23	0.18	0.21	0.59	0.18	0.32	0.32	0.34	0.26	0.31	0.28	0.23	0.14	0.23	0.32	0.36	0.27	0.16	0.37	0.3
Hf	0.60	0.20	0.80	1.00	0.3	0.3	0.4	0.1	1.30	1.30	0.90	1.40	0.50	1.20	0.90	1.1	1.2	1.3	0.7	0.4
In	0.06	0.02	0.05	0.10	0.029	0.059	0.045	0.012	0.06	0.07	0.07	0.08	0.04	0.08	0.06	0.061	0.049	0.055	0.041	0.083
La	14.90	7.30	26.80	15.60	13.8	24	17.9	<0.5	9.90	10.90	3.50	12.80	3.40	15.00	3.10	4.4	3.2	12.5	7.7	3.1
Li	6.10	6.00	7.10	10.80	7.3	13.6	9.6	0.6	5.50	5.00	11.50	8.70	4.00	6.30	9.20	7.1	6.7	7.2	18.4	4

(Continued)

Table 1. (Continued)

	Changmar Complex								Shyok Volcanics											
	16NU08	16NU09	16NU10	16NU11	17NU38	17NU39	17NU40	17NU35	16NU15a	16NU15b	16NU15c	16NU15d	16NU15e	16NU15f	16NU15g	17NU33	17NU34	17NU36	17NU37	17NU41
Mn	1500.00	490.00	1140.00	2250.00	850	969	1040	1380	1280.00	1410.00	1130.00	1390.00	1210.00	1240.00	1330.00	1420	918	1120	1660	1680
Mo	0.99	0.84	0.99	0.67	0.26	0.33	0.26	0.07	0.70	0.65	0.19	0.71	0.20	1.28	0.42	0.25	0.32	0.22	0.05	0.21
Nb	1.40	1.10	4.10	2.20	1.3	3.6	3.2	0.1	6.80	7.60	3.30	10.00	2.60	12.80	3.00	1.9	1	7.2	1.6	2.8
Ni	12.30	5.10	9.20	19.90	4.3	6.8	8.3	771	39.80	23.60	57.80	24.70	283.00	33.90	368.00	19.3	50.9	57.2	1115	51.1
P	1490.00	1210.00	940.00	1120.00	1710	830	940	30	920.00	1230.00	430.00	1470.00	430.00	1680.00	400.00	360	340	810	450	390
Pb	5.50	8.90	13.80	6.00	7.6	7.1	8.7	<0.5	0.90	0.70	0.50	0.90	<0.5	0.80	1.20	0.6	<0.5	0.7	<0.5	<0.5
Rb	21.00	15.00	118.00	45.20	29.6	95.9	91.5	0.1	11.60	14.60	1.80	9.20	37.30	16.80	9.60	2.1	0.3	0.9	4	0.6
Re	<0.002	<0.002	<0.002	<0.002	0.002	0.003	0.003	0.007	<0.002	<0.002	<0.002	<0.002	<0.002	<0.002	<0.002	<0.002	0.003	<0.002	<0.002	0.002
Sb	0.15	0.29	0.61	0.80	0.23	0.8	0.43	0.18	0.33	0.18	0.08	0.14	<0.05	0.08	0.08	0.12	0.12	0.31	0.14	0.17
Sc	30.60	6.70	22.60	62.50	14.5	24.6	23	11.9	30.20	32.70	40.50	26.50	27.80	26.10	36.00	34.3	33.4	27.5	38.2	46.9
Se	1.00	<1	<1	1.00	<1	<1	<1	<1	1.00	1.00	1.00	1.00	1.00	2.00	1.00	1	1	1	<1	1
Sn	0.50	0.40	1.40	0.90	0.6	0.9	0.8	<0.2	1.00	1.00	0.60	1.20	0.50	1.20	0.70	0.6	0.4	0.8	0.4	0.6
Sr	502.00	771.00	331.00	206.00	483	253	451	5.1	183.00	141.00	137.00	131.50	87.70	137.00	157.00	52.2	56.2	116	15.7	98.6
Te	<0.05	<0.05	<0.05	<0.05	<0.05	<0.05	<0.05	0.14	<0.05	<0.05	<0.05	<0.05	<0.05	<0.05	<0.05	<0.05	<0.05	<0.05	0.09	<0.05
Th	2.95	1.85	19.35	5.38	5.17	18.65	8.41	0.02	0.79	0.69	0.34	0.87	0.24	1.16	0.30	0.58	0.45	1.19	1.17	0.24
Tl	0.12	0.11	0.38	0.13	0.18	0.29	0.25	0.05	0.04	0.06	<0.02	0.06	0.10	0.09	0.03	0.05	<0.02	<0.02	0.02	<0.02
U	0.60	0.50	2.50	1.10	0.9	2.5	1.8	<0.1	0.30	0.30	0.10	0.40	0.10	0.50	0.30	0.2	0.5	0.4	0.3	0.1
V	325.00	123.00	206.00	569.00	103	172	186	41	288.00	281.00	306.00	323.00	207.00	290.00	288.00	321	200	218	144	359
Y	18.00	7.10	25.30	30.20	15.5	26.8	20.6	1.3	22.10	29.20	18.90	30.00	14.30	28.80	16.80	23.1	14.1	22.3	9.3	24.8
Zn	90.00	40.00	79.00	145.00	58	70	75	72	74.00	104.00	85.00	86.00	75.00	110.00	80.00	94	50	72	102	106
Zr	15.80	5.70	13.00	23.80	5.6	5	8	2.6	41.90	44.30	20.80	43.10	11.40	34.60	25.00	34.8	34.9	30.8	19.3	6.6
Dy	3.14	1.44	4.11	4.85	2.91	4.42	3.47	0.22	3.98	4.79	3.03	4.96	2.25	5.11	2.84	3.83	2.43	3.89	1.78	4.17
Er	1.75	0.80	2.42	2.88	1.62	2.56	2.06	0.15	2.15	2.61	1.83	2.71	1.33	2.69	1.68	2.43	1.49	2.15	0.92	2.7
Eu	1.37	0.97	1.10	1.16	1.2	1.24	1.12	0.08	1.55	1.62	0.82	1.91	0.69	1.86	0.87	0.9	0.57	1.23	0.45	0.93
Gd	3.32	1.52	4.34	4.76	3.43	4.66	3.71	0.18	3.93	4.46	2.45	4.84	1.93	5.05	2.34	3.14	2.14	3.63	2.13	3.36
Ho	0.62	0.28	0.84	0.99	0.6	0.87	0.7	0.05	0.80	0.96	0.64	0.99	0.46	1.00	0.57	0.84	0.51	0.77	0.35	0.88
Lu	0.25	0.11	0.37	0.43	0.21	0.37	0.32	0.02	0.23	0.29	0.23	0.29	0.16	0.26	0.22	0.27	0.23	0.23	0.11	0.37
Nd	16.20	8.30	24.80	19.40	17.4	25.2	19.6	0.4	14.30	15.90	6.50	18.40	5.40	19.80	6.30	8.4	5.9	14.1	11.7	7.3
Pr	3.53	1.84	5.82	3.92	3.98	6.14	4.55	0.08	2.91	3.23	1.24	3.74	1.04	4.16	1.20	1.67	1.23	3.28	2.57	1.37
Sm	3.50	1.74	5.07	4.83	3.83	5.41	4.25	0.12	3.47	4.03	2.03	4.36	1.61	4.66	1.87	2.5	1.81	3.46	2.57	2.46
Tb	0.48	0.22	0.62	0.70	0.47	0.68	0.54	0.03	0.57	0.70	0.42	0.75	0.32	0.76	0.39	0.55	0.37	0.6	0.3	0.62
Tm	0.26	0.12	0.37	0.43	0.23	0.39	0.32	0.02	0.30	0.37	0.28	0.38	0.20	0.36	0.25	0.35	0.23	0.3	0.12	0.39
Yb	1.68	0.74	2.44	2.94	1.45	2.49	2.02	0.15	1.78	2.24	1.71	2.21	1.24	2.13	1.58	2.11	1.55	1.86	0.83	2.61

comparable minimum ages of *c.* 104 Ma for the Shyok Volcanics and *c.* 134 Ma for Chalt Volcanics (Fig. 2; Khan *et al.* 2007; Thanh *et al.* 2012). The volcanic pile of the Southern Group described by Rolland *et al.* (2000) is similar to the Shyok Volcanics and was investigated in the area of Thalle and Muchilu, *c.* 100 km NW along the Shyok Suture from our study area. These basalt-basaltic andesite lava flows, tuffs and pillowed units of the Southern Group were intruded by the Ladakh Batholith and unconformably overlain by conglomeritic molasse (Rolland *et al.* 2000). These rock relationships match those of the Shyok Valley and Saltoro Range (Fig. 1), where the ophiolitic Shyok Volcanics (basalts-basaltic trachyandesites, Table 1) are intruded by the Ladakh Batholith (Fig. 3d, e) and are unconformably overlain by the Saltoro Molasse (Upadhyay *et al.* 1999; Borneman *et al.* 2015). Further west from Thalle, Shyok VA-ophiolite-related rocks within the Shyok Suture were documented by Robertson & Collins (2002) where, in addition to pillow basalts and ultramafic rocks, the radiolarian cherts and volcanoclastic sandstones were found in the Tectonic Mélange near Shigar in Pakistan, *c.* 130 km NW from our study area. These lithological descriptions from Pakistan are consistent with those along the Shyok Valley, and probably represent different elements of the same volcanic-arc ophiolite that was dismembered along the Shyok Suture.

A further *c.* 300 km W–NW from our study area near Gilgit, the Matum Das tonalite along the Shyok Suture in Pakistan is the oldest intrusive rock found within the Kohistan Arc (Schaltegger *et al.* 2003; Jagoutz *et al.* 2018). The Matum Das tonalite could be related to the Changmar Complex rocks from the Nubra region (Fig. 2). In the Kohistan region, the basaltic Chalt Volcanics are intruded by the Matum Das, and both formations are stitched by the Kohistan Batholith (Fig. 2; Petterson & Windley, 1985). Similarly, in the Nubra region, the Shyok Volcanics, which are considered to be related to the Chalt Volcanics (Thanh *et al.* 2012), are intruded by the Changmar Complex; both formations are stitched by the Ladakh Batholith, which has many basaltic xenoliths of the Shyok Volcanics or Changmar Complex (Figs 2, 3). The Matum Das tonalite is deformed and cross-cut by the basic and undeformed Jutal dykes (Coward *et al.* 1982; Petterson & Windley, 1985). The Rb–Sr isochron dating of the Matum Das yielded an age of *c.* 102 Ma and ^{40}Ar – ^{39}Ar dating of the Jutal dykes an age of *c.* 75 Ma. This original geochronology and field relationships are used to bracket the collision of the Kohistan Arc with Eurasia (Petterson & Windley, 1985), but the age of the tonalite has been extended to Late Jurassic (Schaltegger *et al.* 2003; Jagoutz *et al.* 2018).

3. Field relationships

We investigated outcrops of the Shyok VA-ophiolite rocks along the Shyok Suture in the Nubra region along the Diskit–Turtuk Highway from Hundar to Turtuk. We named the newly discovered intrusive suite the Changmar Complex, after the nearby village of Changmar that lies in the middle of this unit (Fig. 1). The Changmar Complex is composed of norites, gabbronorites, plagiogranites, harzburgites and serpentinites. These units are intrusive amongst each other; for example, a plagiogranite intrudes the surrounding gabbronorite (Fig. 3a). This complex extends between Bogdang and Skuru villages, measuring *c.* 15 km along NW–SE strike (Fig. 1). Its width is approximately 12 km in an E–W direction, where its eastern exposure extent is marked by the Shyok River and the Shyok Volcanics are exposed on the opposite riverbank (Fig. 1). The original contact between the Changmar Complex and Shyok

Volcanics is not exposed as the alluvial fans are covering the contact. The contact is now faulted, but the original relationship was probably intrusive into the volcanic pile or part of the original VA-ophiolite sequence. The western boundary is marked by the Ladakh Batholith, which intrudes the Changmar Complex and Shyok Volcanics, where the granodiorite plutons of the Ladakh Batholith contain mafic xenoliths of these formations (Figs 2, 3d, e). This contact was later modified by the Khalsar Thrust (Fig. 1). The Khalsar Thrust disrupts all contacts in the northern part of the Shyok Valley, where the Changmar Complex and Shyok Volcanics are always in fault contact, and in turn both are a footwall to the Ladakh Batholith (Fig. 1).

Depicted in Figure 3 are the sampled outcrops from the northern part of the Shyok Valley; their global positioning system locations are provided in Table 1. Gabbronorite and plagiogranite samples 16NU08 and 16NU09 were collected from a large slab on the side of the road that broke off the adjacent cliff face just 10 m away (Fig. 3a) at the road sign indicating 6 km to Changmar. This outcrop reveals an intrusive relationship between the dominant coarse-grained gabbronorite and younger plagiogranite. The plagiogranite displays a minor chilled margin, and a small amount of chalcopyrite mineralization in the gabbronorite is present along the contact. Field mapping of the ranges above the Diskit–Turtuk Highway established the presence of the harzburgite bodies (Table 1). The contact is interpreted to be intrusive (gabbronorites-plagiogranites intruding the harzburgite); however, the exact nature of the contact could not be established at this locality due to minimal exposure caused by an extensive alluvial sediment cover. The contact between the gabbroic rocks and harzburgite shows signs of serpentinization.

The outcrop of the Shyok Volcanics shown in Figure 3b, c was found in the northern Shyok Valley near the village of Bogdang (Fig. 1), and is the location of samples 16NU15a–g (co-ordinates provided in Table 1 and Fig. 3). In this part of the valley the Shyok Volcanics are less deformed in comparison to the schistose outcrops near Diskit and Hundar (Fig. 1). Pillow basalts are common (Fig. 3b), and other basalts are massive with minor limestone lenses (Fig. 3c). Other than thin carbonate lenses within the basalts, no other sedimentary or volcanoclastic rocks were found among exposures between Skuru and Bogdang villages (Fig. 1).

4. Analytical methods

4.a. Major and trace elements

Weathered surfaces or fracture-affected material was cut off from the collected samples in order to obtain unaltered rock interior. Approximately 100 g of the fresh rock was crushed using Tungsten Carbide ring grinder (TEMA). For trace-element analysis, 5 g of rock powder was mixed with polyvinyl acetate (PVA) and fused into buttons in aluminium cups, dried for at least 12 hours in an oven at a temperature of 60°C, and then analysed using SPECTRO XEPOS X-ray fluorescence (XRF) spectrometer at University of Wollongong. The same instrument was used to conduct major-element analysis, for which rock powders were fused with 12% tetraborate and 22% metaborate flux to produce glass buttons used in the analysis.

Rare earth elements (REEs) and other trace elements were analysed using inductively coupled plasma mass spectrometry (ICP-MS) at ALS Minerals Division, Brisbane (geochemical procedure ME-MS61r). A pulverized sample was added to lithium metaborate/lithium tetraborate flux and fused in a furnace to form

Table 2. Summary of SHRIMP U–Pb ages (Ma) of zircons from the gabbro-norite and plagiogranite of the Changmar Complex. Abbreviations: b – broad zoned; e – end; fr – fragment; h – homogeneous; hd – homogeneous dark, low luminescence; m – middle; osc – oscillatory zoned; p – prism; r – rounded by abrasion.

Labels	Site	U (ppm)	Th (ppm)	Th/U	f206 (%) ^a	²³⁸ U/ ²⁰⁶ Pb ^b ± 1σ	²⁰⁷ Pb/ ²⁰⁶ Pb ^b ± 1σ	²⁰⁶ Pb/ ²³⁸ U ^b ± 1σ
16NU08 Gabbro-norite								
1.1	fr, e, osc	286	181	0.63	0.19	40.59 ± 0.55	0.0485 ± 0.0049	156.9 ± 2.1
2.1	fr, m, osc	795	857	1.08	0.00	40.31 ± 0.48	0.0489 ± 0.0014	158.0 ± 1.9
3.1	fr, m, osc	886	879	0.99	0.13	39.77 ± 0.47	0.0501 ± 0.0014	160.1 ± 1.9
4.1	fr, m, b	720	736	1.02	0.11	39.67 ± 0.47	0.0484 ± 0.0100	160.5 ± 1.9
5.1	fr, m, osc	1814	1907	1.05	0.09	39.71 ± 0.45	0.0500 ± 0.0009	160.3 ± 1.8
6.1	fr, m, b	699	493	0.71	0.07	40.17 ± 0.48	0.0486 ± 0.0026	158.5 ± 1.9
7.1	fr, m, osc	824	568	0.69	0.10	39.97 ± 0.47	0.0485 ± 0.0019	159.3 ± 1.9
8.1	fr, m, osc	1326	1272	0.96	0.86	39.54 ± 0.46	0.0521 ± 0.0024	161.0 ± 1.8
9.1	fr, m, osc	1304	1387	1.06	0.03	39.98 ± 0.46	0.0489 ± 0.0013	159.3 ± 1.8
10.1	fr, m, osc	986	1092	1.11	0.10	39.90 ± 0.47	0.0492 ± 0.0016	159.6 ± 1.8
11.1	fr, m, osc	1018	1234	1.21	0.05	39.97 ± 0.46	0.0484 ± 0.0017	159.3 ± 1.8
12.1	fr, m, osc	1425	1922	1.35	0.06	40.37 ± 0.46	0.0490 ± 0.0012	157.8 ± 1.8
16NU09 Plagiogranite								
1.1	fr, m, osc	1679	1585	0.94	0.01	40.43 ± 0.46	0.0488 ± 0.0013	157.5 ± 1.8
2.1	p, m, osc	1381	1282	0.93	0.04	40.11 ± 0.46	0.0480 ± 0.0015	158.8 ± 1.8
3.1	fr, e, osc	1674	1947	1.16	0.06	40.19 ± 0.46	0.0491 ± 0.0011	158.4 ± 1.8
4.1	fr, e, b	2340	2335	1.00	−0.01	40.04 ± 0.45	0.0488 ± 0.0009	159.0 ± 1.8
5.1	fr, e, osc	719	715	0.99	0.10	40.45 ± 0.48	0.0502 ± 0.0014	157.4 ± 1.8
6.1	fr, e, osc	1350	1377	1.02	0.13	40.13 ± 0.46	0.0504 ± 0.0010	158.7 ± 1.8
7.1	fr, m, osc	775	894	1.15	0.10	40.87 ± 0.49	0.0490 ± 0.0018	155.8 ± 1.8
8.1	fr, m, osc	1085	973	0.90	−0.01	40.05 ± 0.47	0.0475 ± 0.0018	159.0 ± 1.8
9.1	fr, e, b	852	851	1.00	0.14	42.78 ± 0.51	0.0492 ± 0.0018	149.0 ± 1.8
10.1	fr, e, osc	738	730	0.99	0.08	41.59 ± 0.50	0.0488 ± 0.0019	153.2 ± 1.8
11.1	fr, m, osc	1010	971	0.96	0.14	42.21 ± 0.50	0.0494 ± 0.0016	150.9 ± 1.8
12.1	fr, e, osc	1710	1825	1.07	0.01	41.99 ± 0.48	0.0488 ± 0.0011	151.7 ± 1.7

^af206 (%) is the amount of ²⁰⁶Pb modelled as non-radiogenic, based on measured ²⁰⁴Pb.

^bCorrected for common Pb using measured ²⁰⁴Pb and Cumming & Richards (1975) common Pb composition for likely age of rock.

beads. Each bead is cooled and dissolved in an acid mixture containing nitric, hydrochloric and hydrofluoric acids. The resulting solution is neutralized and diluted before being analysed by ICP-MS. Standards used were OREAS 120 and STSD-1, and results are within a 10% error tolerance. Trace-element data reported in this study are based on ICP-MS results, not the XRF.

Standardized characterization and discrimination of whole-rock geochemical data was carried out using the software GDCKit (Janousek *et al.* 2006).

4.b. U–Pb zircon dating

Zircon grains were extracted by conventional density and isodynamic methods from 3 kg of rock sample. Zircon grain concentrates were handpicked, avoiding grains with abundant mineral inclusions, and *c.* 150 grains from each sample, as well as 20 grains of the standards TEMORA-2 (Black *et al.* 2004) and 10 grains of OG1 (Stern *et al.* 2009), were cast into an epoxy resin mount. The

encapsulated grains were ground to expose a middle section through the majority of the grains, and then polished with 1 μm diamond paste. The mount was mapped using reflected light and cathodoluminescence (CL) imaging. The U–Pb zircon dating was carried out at the Australian National University (ANU) in Canberra using the SHRIMP RG instrument. Analytical procedures followed those described by Williams (1998). The analytical spot size was *c.* 20 μm. Raw data were reduced using the ANU new data reduction software ‘POXI-SC’. The ²⁰⁶Pb/²³⁸U ratio of unknowns was calibrated using measurements of TEMORA-2 (U–Pb ages concordant at 417 Ma; Black *et al.* 2004) undertaken after every third analyses of unknowns; standard results are reported in online Supplementary Table S1 (available at <http://journals.cambridge.org/geo>). U and Th abundance was calibrated using measurement of the reference zircon SL13 (U = 238 ppm) located in a set-up mount. The reduced and calibrated data were assessed and plotted using the ISOPLOT Excel™ software add-in of Ludwig (2008), and finalized results are presented in Table 2.

4.c. Lu–Hf isotopic analysis

Zircon Lu–Hf isotopic measurements were conducted on the Research School of Earth Sciences, ANU ThermoFinnigan Neptune multi-collector (MC) ICP-MS coupled to a 193 nm ArF excimer laser fitted with a HelEx He atmosphere ablation cell using methods as described in Hiess *et al.* (2009). The laser pulsed at 5 Hz with an energy density of 10 J cm^{-2} , and the samples were ablated using a $42 \times 42 \text{ }\mu\text{m}$ square spot. A gas blank and a suite of five reference zircons with varying REE contents (Monastery, Mud Tank, FC1, Plesovice and QGNG) were analysed after every 10–15 unknown sample spots throughout the session as quality control monitors. The mass spectrometer intensity and peaks were tuned with NIST SRM 610 glass, which has *c.* 450 ppm of Hf. Typical ^{178}Hf signal intensity at the start of ablation on the zircons was 4 V. An array of nine Faraday cups was set up in a static collection scheme. Complete Lu–Hf isotopic analyses for the samples are presented in Table 3 and results for the reference zircons analysed in the same session can be viewed in online Supplementary Table S2 (available at <http://journals.cambridge.org/geo>). Details of instrument set-up for the session are also given in Table S2.

5. Results

5.a. Petrography

The gabbro sample sampled for dating (16NU08) displays slight grain alignment in outcrop which can also be seen under the microscope. It consists of plagioclase (60%), clinopyroxene (22%), orthopyroxene (15%), trace quartz and accessory ilmenite, magnetite and apatite (Fig. 4a, b). It is holocrystalline, with equigranular medium grain texture. A hypidiomorphic crystal texture is observed, where Fe-rich phases (clinopyroxene and orthopyroxene) show signs of disequilibrium/re-absorption with later felsic phases (plagioclase and quartz) as evident by the rounded crystal shape, reaction/alteration coronas and embayments. In contrast, plagioclase is euhedral with characteristic lamellar multiple-twinning textures, with some crystals showing zonation. Quartz is rare and occurs interstitially between other silicates; it is almost exclusively associated with plagioclase (Fig. 4a, b). Zircon crystals are observed within these quartz intergranular fillings. Evidence of minor alteration is observed along grain boundaries and microfractures in the form of sericitization of plagioclase and chloritization of pyroxenes.

A plagiogranite sample (16NU09) from the rock intruding the gabbro (Fig. 3c) displays clear crystal alignment. This plagiogranite consists of plagioclase (80%), biotite (5%), amphibole (4%), muscovite (3%), chlorite (2%), quartz (2%) and accessory ilmenite, magnetite and apatite. It displays a holocrystalline porphyritic texture, dominated by plagioclase which is subhedral to euhedral. This sample shows signs of hydrothermal alteration with pyroxenes and amphiboles being extensively replaced and broken down to biotite and chlorite, as well as accessory second-generation iron oxide (Fig. 4c). Plagioclase shows signs of alteration in the form of dusty texture and sericitization. Quartz exists in interstitial form, filling intergranular space between other silicates. Another plagiogranite sample (16NU10) shows very similar composition and textures to 16NU09, but with higher quartz content and lesser alteration (Fig. 4d).

Harzburgite sample (17NU35) is altered to serpentinite and no unaltered primary minerals remain. However, thin-section petrography reveals that serpentine and chlorite has pseudomorphed olivine, which dominated the primary mineralogy (Fig. 4e). Small

altered phenocrysts of orthopyroxene are observed and minor tremolite occurs as a high-temperature alteration phase. The olivine pseudomorphs are studded with small grains of opaque minerals (magnetite) within the crystals and along the fractures, a by-product of the serpentinization reaction.

Sample 16NU15a is representative of the massive basalts that make up the bulk of the Shyok Volcanics (Fig. 4f). It is aphanitic and green in appearance as a result of chlorite alteration associated with greenschist facies metamorphism. In thin-section, randomly orientated microcrysts of plagioclase are the only primary mineral left unaltered from the original protolith. Other primary minerals and glass matrix have been altered to chlorite and sericite (Fig. 4f).

5.b. Whole-rock major- and trace-element geochemistry

Geochemical results are presented in Table 1. The intrusive Changmar Complex is composed of gabbro and plagiogranites with SiO_2 values ranging between 50 and 57%, with relatively low MgO (1.4–4.5%), variable Fe_2O_3 (4.6–11%), low–moderate CaO (3.8–11%) and low TiO_2 (0.4–0.8%) values. The K_2O content varies between 1.2 and 3.7%, and Na_2O between 2.4 and 4.6%. The observed major-element variation is attributed to evolving magma composition. Light REEs (LREEs) are enriched relative to heavy REEs (HREEs) ($3.2 < \text{Ce}_N/\text{Yb}_N < 6.3$; Fig. 5a). On the normal mid-ocean-ridge basalt (N-MORB) normalized plots the Changmar Complex rocks display well-defined Nb- and Ti-negative anomalies and strong Pb- and Sr-positive anomalies, suggesting an origin in a supra-subduction zone (SSZ) setting (e.g. Pearce, 1982). The geochemistry data for the Matum Das tonalite (Jagoutz *et al.* 2018) from the Kohistan Arc has been plotted for comparison with the Changmar Complex rocks (Fig. 5). Both rock formations are of Late Jurassic age and have similar subduction-zone-related geochemistry patterns; they are therefore suggested to be related in terms of their tectonic setting. However, the degree of LREE and large-ion lithophile element (LILE) enrichment is higher for the Changmar Complex. On the Ti/V plot of Shervais (1982) the Changmar Complex samples plot between Ti/V 10 to 20 ratios and within the array for typical volcanic-arc ophiolites in the subduction-related ophiolite compilation of Dilek & Furnes (2011). The harzburgite sample from the Changmar Complex displays a slight positive Eu anomaly and Lu-depletion on an N-MORB-normalized plot (Fig. 5b). The N-MORB-normalized trace-element plot shows distinctly parallel patterns between the gabbroic rocks and harzburgite, suggesting that the latter represents an early cumulate phase rather than the residual mantle peridotite from which melts were extracted. On the Nb/Yb–Th/Yb plot of Pearce (2008), the Changmar Complex intrusive rocks plot as a cluster within the volcanic-arc array (Fig. 5d).

The Shyok Volcanics are predominantly basaltic, with SiO_2 values ranging between 44 and 51%, with highly variable MgO (4.7–19%), variable Fe_2O_3 (7.5–14%), highly variable CaO (2.6–12.4%) and moderate TiO_2 (0.4–2.1%) values. The K_2O content varies between 0.05 and 1.1%, and Na_2O between 0.5 and 5.5%. Sample 16NU15e was excluded from major-element data interpretation due to observed calcite veining within it. Our petrographic examination has revealed that the Shyok Volcanics have been affected by sericitization and chloritization and, for this reason, we characterize these rocks using only the trace elements that are immobile and remain unaffected by these processes (e.g. Ward *et al.* 1992). On the chondrite-normalized plot (Fig. 5a) the Shyok Volcanics split into two subgroups: the LREE/HREE non-

Table 3. Lu–Hf isotopic results summary for SHRIMP-dated zircons from gabbro-norite and plagiogranite^a of the Changmar Complex. SE – standard error.

Spot	¹⁷⁴ Hf/ ¹⁷⁷ Hf	1SE	¹⁷⁸ Hf/ ¹⁷⁷ Hf	1SE	¹⁷⁶ Lu/ ¹⁷⁷ Hf	1SE	¹⁷⁶ Hf/ ¹⁷⁷ Hf	1SE	$\epsilon_{\text{Hf}(t)}$	U/Pb age (Ma)	Initial ¹⁷⁶ Hf/ ¹⁷⁷ Hf	$\epsilon_{\text{Hf}(t)}$	T_{DM} (Ga)
16NU08 Gabbro-norite													
1.1	0.008655	0.000009	1.467521	0.000031	0.000532	0.000008	0.283120	0.000008	11.85	157	0.28312	15.3	0.181
2.1	0.008643	0.000009	1.467404	0.000026	0.001483	0.000025	0.283117	0.000008	11.76	158	0.28311	15.1	0.190
3.1	0.008643	0.000009	1.467402	0.000026	0.001485	0.000025	0.283117	0.000008	11.73	158	0.28311	15.1	0.191
4.1	0.008646	0.000009	1.467408	0.000030	0.001363	0.000006	0.283129	0.000009	12.15	161	0.28312	15.6	0.173
5.1	0.008655	0.000012	1.467577	0.000028	0.001457	0.000011	0.283152	0.000013	12.97	160	0.28315	16.4	0.141
6.1	0.008668	0.000011	1.467459	0.000026	0.001266	0.000011	0.283134	0.000009	12.34	159	0.28313	15.7	0.165
5.1	0.008651	0.000014	1.467663	0.000034	0.001621	0.000026	0.283168	0.000011	13.55	160	0.28316	16.9	0.118
7.1	0.008665	0.000010	1.467428	0.000026	0.001993	0.000021	0.283142	0.000009	12.63	159	0.28314	16.0	0.156
8.1	0.008648	0.000008	1.467437	0.000027	0.000603	0.000010	0.283143	0.000007	12.67	161	0.28314	16.2	0.149
9.1	0.008671	0.000008	1.467439	0.000025	0.000328	0.000002	0.283154	0.000007	13.06	159	0.28315	16.6	0.133
9.1R	0.008653	0.000010	1.467473	0.000033	0.000921	0.000005	0.283142	0.000010	12.61	159	0.28314	16.0	0.153
10.1	0.008631	0.000010	1.467449	0.000030	0.001179	0.000021	0.283117	0.000008	11.76	160	0.28311	15.2	0.188
11.1	0.008655	0.000012	1.467489	0.000036	0.001979	0.000048	0.283129	0.000009	12.17	159	0.28312	15.5	0.175
12.1	0.008620	0.000015	1.467568	0.000041	0.002338	0.000016	0.283113	0.000014	11.60	158	0.28311	14.9	0.201
B ^b	0.008667	0.000013	1.467506	0.000029	0.001237	0.000003	0.283144	0.000010	12.69	159	0.28314	16.1	0.151
C ^b	0.008671	0.000011	1.467475	0.000025	0.001589	0.000064	0.283140	0.000009	12.57	159	0.28314	15.9	0.157
E ^b	0.008581	0.000016	1.467661	0.000047	0.001927	0.000062	0.283119	0.000011	11.80	159	0.28311	15.1	0.190
E ^b	0.008581	0.000016	1.467661	0.000047	0.001927	0.000062	0.283119	0.000011	11.80	159	0.28311	15.1	0.190
16NU09 Plagiogranite													
1.1	0.008678	0.000010	1.467449	0.000027	0.002766	0.000011	0.283160	0.000008	13.25	158	0.28315	16.5	0.134
2.1	0.008668	0.000013	1.467484	0.000031	0.001976	0.000076	0.283131	0.000011	12.23	159	0.28313	15.6	0.173
3.1	0.008649	0.000010	1.467411	0.000023	0.002791	0.000022	0.283126	0.000010	12.04	158	0.28312	15.3	0.184
4.1	0.008641	0.000008	1.467510	0.000032	0.001068	0.000027	0.283126	0.000010	12.05	159	0.28312	15.5	0.176
5.1	0.008637	0.000010	1.467461	0.000032	0.001571	0.000049	0.283116	0.000010	11.71	157	0.28311	15.0	0.192
6.1	0.008655	0.000008	1.467480	0.000028	0.000995	0.000030	0.283133	0.000008	12.30	159	0.28313	15.7	0.165
7.1	0.008629	0.000009	1.467488	0.000028	0.001401	0.000022	0.283119	0.000010	11.80	156	0.28311	15.1	0.188
8.1	0.008646	0.000012	1.467623	0.000032	0.000748	0.000003	0.283150	0.000011	12.90	159	0.28315	16.4	0.141
9.1	0.008665	0.000014	1.467549	0.000041	0.001777	0.000024	0.283155	0.000013	13.10	149	0.28315	16.2	0.136
10.1	0.008647	0.000010	1.467443	0.000025	0.001440	0.000025	0.283116	0.000008	11.69	153	0.28311	14.9	0.192
11.1	0.008661	0.000011	1.467469	0.000032	0.002088	0.000057	0.283138	0.000009	12.48	151	0.28313	15.6	0.163
12.1	0.008633	0.000012	1.467500	0.000036	0.002056	0.000002	0.283133	0.000012	12.32	152	0.28313	15.5	0.169
A ^b	0.008657	0.000010	1.467536	0.000037	0.001336	0.000022	0.283136	0.000010	12.40	151	0.28313	15.6	0.163
B ^b	0.008619	0.000013	1.467518	0.000052	0.001447	0.000005	0.283130	0.000009	12.19	151	0.28313	15.4	0.172
C ^b	0.008682	0.000017	1.467513	0.000042	0.001958	0.000075	0.283172	0.000012	13.70	151	0.28317	16.9	0.112
D ^b	0.008649	0.000009	1.467453	0.000024	0.001600	0.000018	0.283118	0.000008	11.79	151	0.28311	15.0	0.189

^aReference materials used: FC-1, QNGG, Monastery, Mud Tank (Woodhead & Hergt, 2005) and Plešovice (Sláma *et al.* 2008); see online Supplementary Table S2.

^bAnalysis conducted on zircons which do not have U–Pb age, MSWD age of the rock sample was used to determine initial $\epsilon_{\text{Hf}(t)}$ values for these zircons; ϵ_{Hf} calculated using CHUR values from Bouvier *et al.* (2008); depleted mantle model ages calculated using estimates of $^{176}\text{Hf}/^{177}\text{Hf} = 0.283251$ and $^{176}\text{Lu}/^{177}\text{Hf} = 0.0389$ for the modern upper mantle.

differentiated ($0.9 < \text{Ce}_N/\text{Yb}_N < 1.6$) and LREE/HREE enriched ($3.1 < \text{Ce}_N/\text{Yb}_N < 6.3$; median = 3.8). The non-differentiated group consists of the following samples: 16NU15c, 16NU15e, 16NU15g, 17NU33, 17NU34 and 17NU41; the enriched group consists of samples of 16NU15a, 16NU15b, 16NU15d, 16NU15f, 17NU36 and 17NU37. On the Ti/V plot of Shervais (1982) the non-differentiated

group plots between 10 and 20 ratios along with the Changmar Complex. The enriched group (except 17NU37) plots between 20 and 50 ratios and within the SSZ ophiolite field, out of the volcanic-arc ophiolite array (Fig. 5c). Both groups contain 16NU15a–g samples which were sampled along a 50-m stratigraphically coherent and continuous outcrop; the array of samples from this outcrop

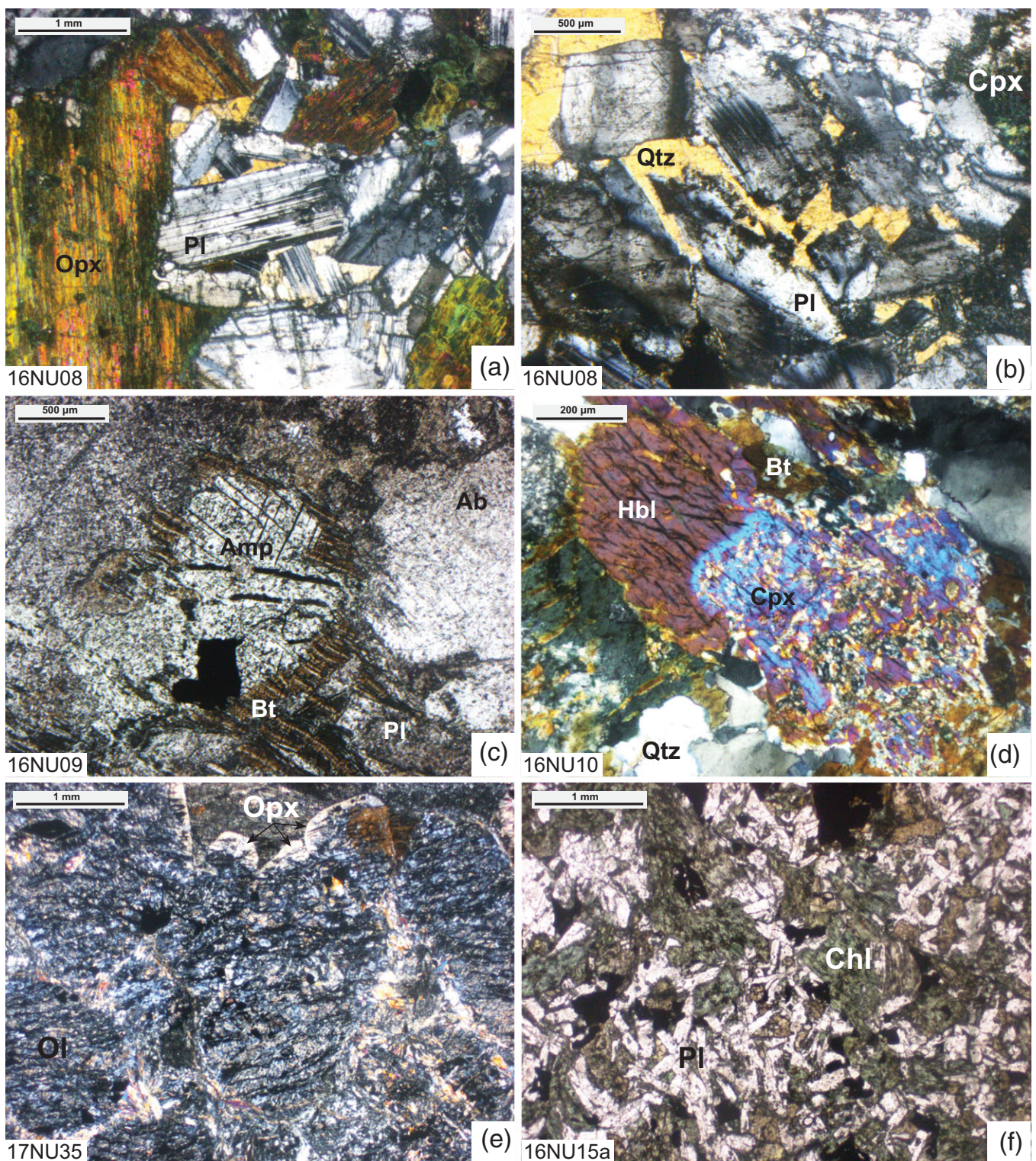


Fig. 4. (Colour online) Petrographic microphotographs of thin-sections from samples investigated in this study. Abbreviation nomenclature is from Kretz (1983). (a, b) Gabbro 16NU08 showing coarse grain composition, defined by euhedral plagioclase and pyroxenes. Interstitial quartz can be seen on both photographs, but it is not common. (c) Plagiogranite 16NU09 showing strong alteration, evident by dusty texture and breakdown of amphibole into biotite; (d) Plagiogranite 16NU10 showing breakdown of clinopyroxene to hornblende. Quartz content is higher than in 16NU09. (e) Harzburgite 17NU35 preserving olivine morphology, but has completely been converted into secondary products, mainly chlorite. (f) Basalt of the Shyok Volcanics (16NU15a) showing high plagioclase content, whereas rest of the Fe-rich phases have altered into chlorite.

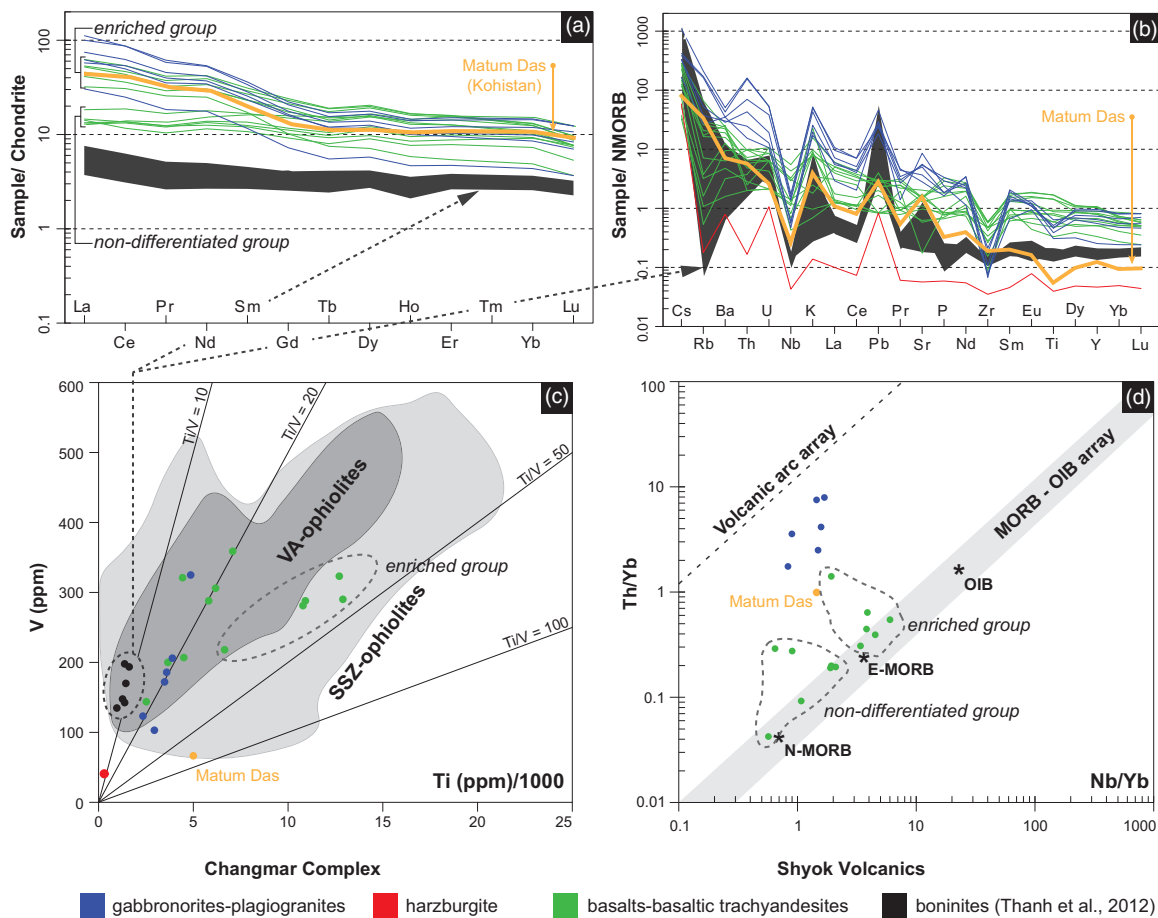


Fig. 5. (Colour online) Whole-rock geochemical plots for the Changmar Complex and Shyok Volcanics, as well as boninites from the Shyok Volcanics shown as the black fields on plot (a) and (b), adopted from Thanh *et al.* (2012). Data for the Matum Das tonalite from Jagoutz *et al.* (2018). (a) REE concentrations for the Shyok VA-ophiolite samples normalized to chondrite after Sun & McDonough (1989). (b) Trace-element distribution, data normalized to N-MORB after Sun & McDonough (1989). (c) Ti/V plot of Shervais (1982) showing samples analysed in this study and boninites from the study of Thanh *et al.* (2012). The encircled are the Shyok Volcanics samples from the enriched group (see Results), whereas the remaining samples belong to non-differentiated group (except 17NU37, which plots next to the boninite group). The VA-ophiolites and SSZ-ophiolites shaded fields represent data distribution for corresponding ophiolite types from the global ophiolite survey of Dilek & Furnes (2011). Note that the SSZ-ophiolites field includes back-arc, fore-arc and oceanic back-arc subtype ophiolites. (d) Nb/Yb v. Th/Yb plot of Pearce (2008) showing results for the Changmar Complex and Shyok Volcanics. The samples from the latter are circled based on the subgrouping in plot (a) (see Section 5.b).

therefore points to the magma heterogeneity rather than long-term ophiolite evolution. Normalized to N-MORB, the Shyok Volcanics display negative Nb and Zr anomalies, and slightly positive Pb and Sr anomalies. Such characteristics along with the LREE and LILE enrichments are consistent with the supra-subduction zone basalts (Fig. 5b; Pearce, 1982). The Shyok Volcanics spread across the N-MORB and E-MORB fields on the Nb/Yb–Th/Yb plot of Pearce (2008) and display a Th-enrichment-driven shift into the volcanic-arc array (Fig. 5d), which is consistent with a subduction-zone-related environment.

5.c. U–Pb–Hf zircon geochronology

SHRIMP U–Pb zircon dating results for the gabbro-norite (16NU08) and plagiogranite (16NU09) are reported in Table 2. The ^{204}Pb -corrected ratios are plotted on Tera–Wasserburg concordia diagrams (Fig. 6). Zircon grains from both the gabbro-norite and plagiogranite samples were analysed using laser ablation (LA) -MC-ICP-MS to determine their initial ε_{Hf} values which are presented in Table 3. The Lu–Hf analyses were conducted directly over all the U–Pb dating sites with four additional sites on non-dated zircons, producing 16 analyses per sample.

Zircons from the gabbro-norite (16NU08) show clear oscillatory and broad zoning (Fig. 7), with a Th/U ratio range of 0.63–1.35. All analyses yielded a weighted mean $^{206}\text{Pb}/^{238}\text{U}$ age of 159.3 ± 0.8 Ma (MSWD = 1.6; $n = 12$) without rejection of any data (Fig. 6a). If the spread beyond analytical error was modelled as to the result of a small amount of radiogenic Pb loss, a single grain (spot 4.1) was excluded and the remaining 11 analyses agreeing within error yield a weighted mean age of 159.4 ± 0.9 Ma (MSWD = 0.5; $n = 11$), which we interpret as the crystallization age for the gabbro-norite. The gabbro-norite zircons show highly depleted ε_{Hf} (t) signatures ranging from +14.9 to +16.9 (Fig. 8; Table 3), in accordance with estimated depleted mantle compositions and indicating a juvenile mantle as the sole magma source.

Zircons from the plagiogranite (16NU09) show similar characteristics to the gabbro-norite zircons, but oscillatory zoning is more common (Fig. 7) and their Th/U ratio range is 0.9–1.16. The zircons yielded a distinctly bimodal $^{206}\text{Pb}/^{238}\text{U}$ age distribution (Fig. 6b). Eight grains within the older population yielded a weighted mean $^{206}\text{Pb}/^{238}\text{U}$ age of 158.1 ± 0.9 Ma (MSWD = 1.5). The large MSWD is caused by analysis spot 7.1 with the youngest apparent age of 155.8 ± 1.8 Ma. If this is attributed to minor loss of radiogenic Pb, then the remaining seven analyses yield a weighted mean

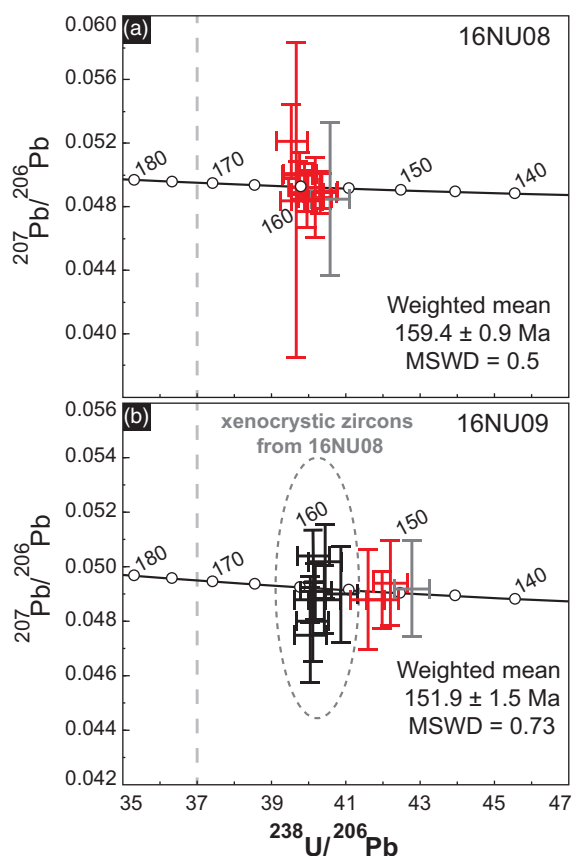


Fig. 6. (Colour online) Tera-Wasserburg concordia diagrams for U-Pb ratios of SHRIMP analysed zircons from (a) gabbronorite and (b) plagiogranite. Red crosses refer to the analysis spots used in age determination, grey to those that were excluded and black to those that are xenocrystic.

$^{206}\text{Pb}/^{238}\text{U}$ age of 158.4 ± 1.1 Ma (MSWD = 0.23). This age is indistinguishable from the 159.4 ± 0.9 Ma age of the gabbronorite host. All four analyses from the younger group of grains, still of magmatic character, yielded a weighted mean $^{206}\text{Pb}/^{238}\text{U}$ age of 151.2 ± 2.8 Ma (MSWD = 3.9; $n = 4$). The large MSWD is caused by analysis 9.1 with the youngest apparent age of 149.0 ± 1.8 Ma. If this is attributed to minor loss of radiogenic Pb, then the remaining three sites yield a weighted mean $^{206}\text{Pb}/^{238}\text{U}$ age of 151.9 ± 1.5 Ma (MSWD = 0.73), which we interpret as the crystallization age for the plagiogranite. The older population is interpreted as xenocrystic grains. Zircons from the plagiogranite also show highly depleted $\varepsilon_{\text{Hf}}(t)$ signatures ranging from +14.9 to +16.9, indicating that the sources of the gabbronorite and plagiogranite, in terms of Hf isotopic composition, are indistinguishable (Fig. 8; Table 3).

6. Discussion

6.a. Shyok VA-ophiolite

The Late Jurassic Changmar Complex (159–152 Ma) represents the oldest recorded magmatic activity within the Shyok Suture in Ladakh. This robust age, coupled with the highly juvenile initial Hf isotopic signature ($\varepsilon_{\text{Hf}} = +14.9$ to +16.9) provides a new and important age for the onset of intra-oceanic island-arc magmatism within the Mesotethys Ocean. The Changmar Complex displays geochemical signatures typical of a mature island-arc setting with high LREE and LILE enrichments (Fig. 5a, b) that are driven by a hydrous melting of a depleted mantle wedge, with the sediment or

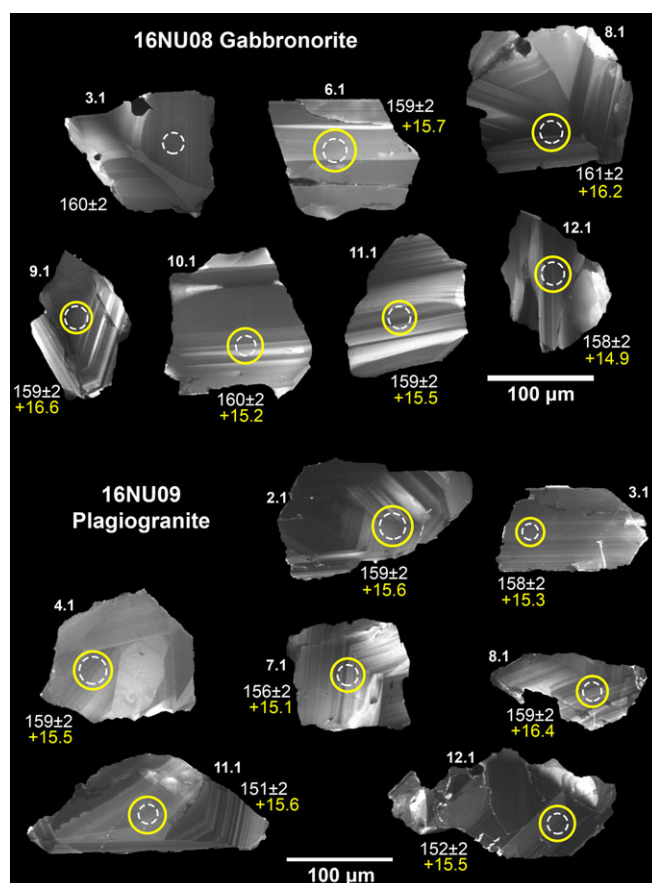


Fig. 7. (Colour online) Zircon plate showing cathodoluminescence images of seven representative zircons from gabbronorite and plagiogranite analysed in this study. White circles indicate SHRIMP analytical spots; yellow circles indicate LA-ICP-MS analytical spots.

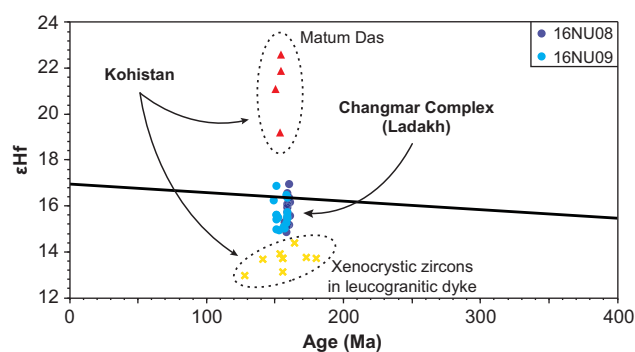


Fig. 8. (Colour online) U-Pb zircon age v. $\varepsilon_{\text{Hf}}(t)$ display of data for the Changmar Complex analysed in this study, and Matum Das tonalite from the Kohistan Arc sourced from Jagoutz *et al.* (2018). Sample 16NU08 is the gabbronorite and 16NU09 is the plagiogranite from the outcrop shown in Figure 3a.

fluid input from a subducting slab into the generated melt (e.g. Dilek *et al.* 2008). The Changmar Complex therefore does not represent a crystalline gabbroic suite of MORB-like oceanic crust, but rather an intrusive complex within a mature intra-oceanic island arc that developed within a supra-subduction zone ophiolitic crust which formed prior to 159 Ma (Late Jurassic).

The Shyok Volcanics from this study display significant LREE and LILE enrichments with negative Nb and Zr anomalies and slightly positive Pb and Sr anomalies, characteristic of supra-

subduction zone magmas (Fig. 5a, b) where sediments or fluids from a subducting slab have contributed to hydrous melt generation (e.g. Pearce, 1982; Dilek *et al.* 2008). The same patterns were observed for the Changmar Complex; however, the degree of LREE and LILE enrichment is lower and more variable in the Shyok Volcanics. Slightly different degrees of the LREE enrichment between the volcanic and intrusive rocks suggest that, while they belong to the same supra-subduction zone arc, they formed during different stages of arc evolution. The lower degree of enrichment in the non-differentiated group of the Shyok Volcanics (Fig. 5a; Section 5.b) suggests less sediment or fluid input into the melt, which could mean these basalts formed during earlier stages of the ophiolite development. These differ from the fore-arc basalts and depleted-fore-arc basalts from recent International Ocean Discovery Program (IODP) Expedition 352 drilling (Reagan *et al.* 2017), which are related to the subduction initiation. The Shyok Volcanics are therefore likely to have formed during the later stages of the ophiolite formation. The enriched group of the Shyok Volcanics and, to a greater degree, the Changmar Complex (Fig. 5a, c; Section 5.b) are likely to represent even later stages of island-arc development, when magmatism progressed into advanced stages of hydrous melt generation above the subduction zone with significant sediment or fluid influences on the melt (e.g. Dilek *et al.* 2008). When plotted on Ti/V discrimination diagram (Shervais, 1982) and compared with the SSZ and VA ophiolites from the global ophiolite survey of Dilek & Furnes (2011), samples from the Shyok Volcanics and Changmar Complex, as well as the boninites from the Shyok Volcanics of Thanh *et al.* (2012), show affinity with the VA ophiolites (Fig. 5c). Together, the Shyok Volcanics and Changmar Complex are interpreted to be discrete elements of a volcanic-arc ophiolite, as defined by Dilek & Furnes (2011), here referred to as the Shyok VA-ophiolite. The Shyok Volcanics have similar geochemical trends and composition to those of the Southern Group from the Skardu area as described by Rolland *et al.* (2000), which also show LREE and LILE enrichments and negative Nb and Ti anomalies. These are likely to be part of the same volcanic-arc ophiolite that was dismembered along the Shyok Suture; however, some elements are not present in the Nubra region. The other rock types expected to be found in typical VA ophiolite such as the sub-aerial more felsic volcanoclastic cover were not identified in this study; however, the Northern Group described by Rolland *et al.* (2000) from the Shyok Suture near Skardu are more evolved and could represent the upper crustal part of the VA ophiolite not identified in the Nubra region.

The Changmar Complex pre-dates all previous formation ages for the Shyok VA-ophiolite and the Kohistan Arc; the new age of 159 Ma therefore provides an older minimum age for the formation of the Shyok VA-ophiolite. The intrusive rocks of this complex represent a well-developed island arc, which means the initiation of this arc system must have occurred prior to this date. The highly positive initial zircon ϵ_{Hf} values of +14.9 to +16.9 from the Changmar Complex (Table 3; Fig. 8) reveal that the magma was juvenile and purely mantle-derived without continental crust contribution. The Changmar Complex from the Shyok VA-ophiolite therefore formed in an intra-oceanic island-arc setting prior to Late Jurassic time, and was remote from the continental crust influences of Eurasia or Lhasa terrane.

6.b. Jurassic intra-oceanic arc system

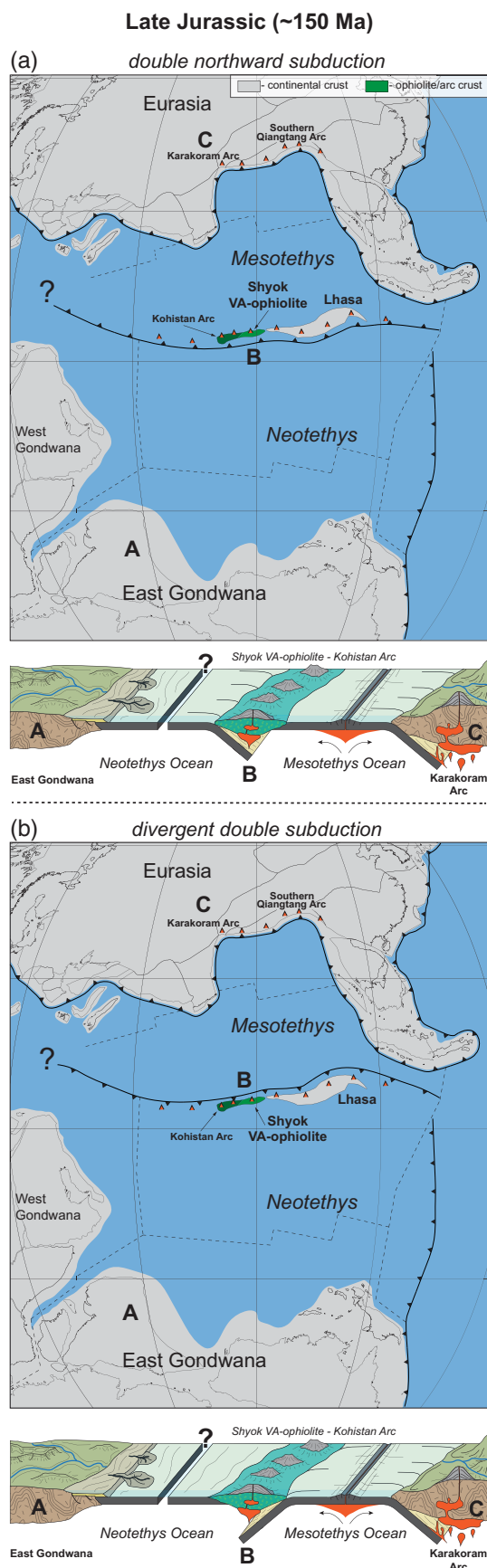
In northern Pakistan, the deformed Matum Das pluton and basic cross-cutting Jutal dykes were originally used to bracket the

collision of the Kohistan Arc with Eurasia (102–75 Ma; Petterson & Windley, 1985). However, its isochron Rb–Sr age of *c.* 102 Ma was recently supplemented by a *c.* 154 Ma age with U–Pb zircon re-dating of the Matum Das (Schaltegger *et al.* 2003; Jagoutz *et al.* 2018). This 154 Ma age provides evidence for an earlier initiation of the Kohistan Arc magmatism (Jagoutz *et al.* 2018), and therefore the initiation of a new Jurassic subduction system within the Tethys Ocean. The U–Pb zircon ages and Hf signatures from the Changmar Complex (159–152 Ma; $\epsilon_{\text{Hf}} = +15$ to +17) are similar to those from the Kohistan Arc (180–128 Ma; $\epsilon_{\text{Hf}} = +13$ to +23), which includes the Matum Das tonalite and xenocrystic zircons in the post-collisional dyke from that region (Fig. 8). The Changmar Complex and the Matum Das tonalite share similar geochemical trends (Fig. 5a, b), that is, a similar degree of LREE to HREE enrichment, a lesser degree but comparable LILE enrichment, negative Nb and Ti anomalies and positive Pb and Sr anomalies (Fig. 5). Both the Changmar Complex and the Matum Das also share comparable field context, as both intruded basaltic volcanic formations, the Shyok Volcanics in Ladakh and the Chalt Volcanics in Kohistan (Fig. 2; Petterson & Windley, 1985). These similarities compel us to suggest that the Changmar Complex and the Matum Das tonalite were part of the same subduction system that formed the Shyok VA-ophiolite and the Kohistan Arc of the Shyok Suture (Fig. 9).

6.c. Subduction polarity, Mesotethys and Shyok–Bangong Suture

One issue that our results cannot reconcile is the polarity of the subduction zone above which the Shyok VA-ophiolite and Kohistan Arc were formed. The original view depicts the northwards subduction of the Neotethys Ocean underneath the oceanic crust of the Mesotethys (the Bangong or Shyok Ocean) forming the intra-oceanic Kohistan Arc while, further to the north, the same overridding oceanic plate was also subducting northwards but beneath southern Eurasia, giving rise to the Karakoram Arc (Fig. 9a; Tahirkheli *et al.* 1979; Bard, 1983; Pudsey, 1986; Coward *et al.* 1987; Robertson & Degnan, 1994; Treloar *et al.* 1996; Searle *et al.* 1999; Jagoutz *et al.* 2018). The original model is valid; however, the same geodynamic realm can be explained by an alternative model.

Coeval magmatism of the Shyok VA-ophiolite, Kohistan Arc and Karakoram Arc can be driven by the divergent double subduction of the Mesotethys oceanic plate (Fig. 9b). This mechanism was postulated in this region by Jan & Asif (1981), Andrews-Speed & Brookfield (1982) and Khan *et al.* (1997), and opposed by Collins *et al.* (1998) and Bignold & Treloar (2003). Khan *et al.* (1997) supported southwards subduction beneath the Kohistan Arc with the progressive increase in high-field-strength element (HFSE) enrichment from north to south, from the Chalt Volcanics to Kamila Amphibolites, a pattern that was found consistent with a modern arc example such as the Izu–Bonin–Marianna Arc (Khan *et al.* 1997). The presence of boninites in the Chalt Volcanics found in the northern part of the Kohistan Arc was further used by Khan *et al.* (1997) to support southwards subduction polarity as a result of their common occurrence in the fore-arc regions. The boninites should not be solely used to infer tectonic setting (Bignold & Treloar, 2003), as they are not entirely limited to fore-arc regions (e.g. Cooper *et al.* 2010). However, a fore-arc origin for the Shyok VA-ophiolite was also inferred from the boninites found within the Shyok Volcanics by Thanh *et al.* (2012), but this fore-arc ophiolitic crust was attributed to the Karakoram Arc. We find this



interpretation unlikely because of the strong juvenile mantle signature ($\epsilon_{\text{Hf}} = +15$ to $+17$) in the ophiolitic rocks that contrasts the Andean-type Karakoram Arc that has an evolved signature ($\epsilon_{\text{Hf}} = -4$ to $+2$; Ravikant *et al.* 2009). The fore-arc ophiolite to continental arc, even evolved, is expected to have some characteristics of a continental-margin-type ophiolite still preserved (see Dilek & Furnes, 2011). These could include subcontinental mantle lehezorite fragments or widespread N-MORBs as a remnant of the continental rifting. Such rocks are not found in the Shyok Suture. It is likely that the Shyok Volcanics represent a fore-arc crust that belonged to an intra-oceanic-arc system (i.e. Shyok VA-ophiolite), rather than a continental arc as clearly demonstrated by the juvenile Hf isotope signatures. In such a tectonic arrangement, the fore-arc rocks of the Shyok Volcanics are better matched with the Chalt Volcanics in Pakistan as suggested by Thanh *et al.* (2012), which are interpreted to be a part of the fore-arc sequence of the Kohistan Arc (e.g. Petterson & Windley, 1991; Khan *et al.* 1997). This correlation favours southwards subduction to form the Shyok VA-ophiolite; however, it does not exclude formation by the northwards subduction as boninites are not restricted to fore-arcs. The mafic rocks from the Shyok Suture were interpreted to originate in arc (e.g. Borneman *et al.* 2015), fore-arc (e.g. Thanh *et al.* 2012) and back-arc environments (e.g. Robertson & Collins, 2002), which highlights the complexity of this suture along-strike. Unfortunately, our results alone cannot reconcile the subduction polarity issue in this geopuzzle; both possibilities are therefore considered feasible (Fig. 9).

A divergent double subduction model is also used to explain the closure of the Mesotethys Ocean and eventual collision between the Qiangtang and Lhasa terranes along the Bangong Suture in Tibet (e.g. Yin & Harrison, 2000; Metcalfe, 2013; Zhu *et al.* 2013, 2016; Kapp & DeCelles, 2019; Li *et al.* 2020). The southwards subduction beneath the Lhasa terrane and coeval northwards subduction beneath the Shyok VA-ophiolite and northwards subduction beneath the Karakoram Arc in Ladakh region. This deductive inference of the south-facing subduction for the formation of the Shyok VA-ophiolite is consistent with previous models that propose a lateral continuation between the Shyok and Bangong sutures, prior to disruption by the Karakoram Fault (Phillips *et al.* 2004; Baxter *et al.* 2009; Robinson, 2009; Borneman *et al.* 2015).

In this geotectonic arrangement, the Mesotethyan terranes such as the Shyok VA-ophiolite, Kohistan Arc and Lhasa were linked by

Fig. 9. (Colour online) Schematic diagrams depicting two possible tectonic models for the closure of the Mesotethys Ocean. Plate reconstruction in Mollweide projection is derived and modified from the GPlates model of Seton *et al.* (2012). The labels A–B–C on the planar view match the tectonic elements depicted in cross-sectional view. (a) Traditional double northwards subduction model (e.g. Tahirkheli *et al.* 1979; Bard, 1983; Coward *et al.* 1987; Robertson & Degnan, 1994; Bignold & Treloar, 2003; Jagoutz *et al.* 2015); and (b) divergent double subduction model (e.g. Soesoo *et al.* 1997), where southwards subduction occurs from west to east beneath the Kohistan Arc and Shyok VA-ophiolite (Jan & Asif, 1981; Andrews-Speed & Brookfield, 1982; Khan *et al.* 1997) and Lhasa (e.g. Zhu *et al.* 2013, 2016) and where concurrently northwards subduction occurs beneath Eurasia, giving rise to the Karakoram Arc (e.g. Searle *et al.* 1999) and Southern Qiangtang Arc (Zhu *et al.* 2016). Palaeolatitude of the Lhasa terrane was adjusted for 150 Ma timeframe using palaeolatitude data from Li *et al.* (2016). Positioning of the mid-ocean ridges and transform faults is hypothetical.

the same Trans-Tethyan subduction system. During the Jurassic Period, these terranes would mark the southern boundary of the seaway tract (Mesotethys Ocean) that is represented by the matched Shyok and Bangong sutures (e.g. Phillips *et al.* 2004; Baxter *et al.* 2009; Robinson, 2009; Liu *et al.* 2014; Borneman *et al.* 2015) rather than matching the Shyok and Yarlung-Tsangpo sutures (cf. Jagoutz *et al.* 2015). This Mesotethyan subduction system might have been responsible for the rifting of the Lhasa terrane from Gondwana during Triassic–Jurassic time and the northwards drift of these terranes to eventually collide with Eurasia (Zhu *et al.* 2011; Li *et al.* 2016). This interpretation is consistent with the timing of the rift and drift of the Lhasa terrane (Li *et al.* 2016), coeval continental-arc magmatism within the Karakoram Arc (162–83 Ma; Heuberger *et al.* 2007; Borneman *et al.* 2015; Groppo *et al.* 2019) and Southern Qiangtang Arc (185–100 Ma; Li *et al.* 2017b; Liu *et al.* 2017) until the collision along the Shyok and Bangong sutures (Li *et al.* 2020). It is also consistent with the diachronous nature of the collision between the Lhasa and Qiangtang terranes (Yan *et al.* 2016; Liu *et al.* 2017). Initiating in the east, this collision would progress westwards along the Bangong suture (125–105 Ma; Yan *et al.* 2016; Li *et al.* 2020) and into the Ladakh region where the Shyok Suture closed at *c.* 92–85 Ma (Borneman *et al.* 2015). It then progress into the Kohistan region, where structural patterns support the diachronous collision (Robertson & Collins, 2002) between the Kohistan Arc and Eurasia along the Shyok Suture at *c.* 90–75 Ma (Petterson & Windley, 1985; Robertson & Collins, 2002).

The Kohistan–Ladakh–Tibet bridging model with the divergent double subduction is favoured because it explains (1) a presence of Jurassic–Cretaceous continental-arc magmatism along the southern boundary of the Karakoram and Qiangtang terranes (Fig. 9b) and (2) coeval magmatic activity within the intra-oceanic Shyok VA-ophiolite and Kohistan Arc and a continental magmatism within the Lhasa terrane (e.g. Zhu *et al.* 2016). Further, (3) it accounts for magmatic shut-off within the Karakoram Arc and Southern Qiangtang Arc during middle–late Cretaceous time due to the Shyok VA-ophiolite and Lhasa terrane collision along the Shyok and Bangong sutures.

The southwards Jurassic Trans-Tethyan subduction system provides a mechanism for the northwards drift of the Lhasa terrane (Zhu *et al.* 2011; Li *et al.* 2016) and, at the same time, it explains the formation of the Shyok VA-ophiolite in Ladakh. The Shyok VA-ophiolite, an intra-oceanic terrane, would have formed in lateral continuity with the Lhasa's northern boundary along the same subduction system (Fig. 9b), but it would be distant and in a different tectonic setting. This was indicated by the Hf isotopic signatures of the Shyok VA-ophiolite (Fig. 8) where, during the Jurassic Period, there was no contribution from an evolved continental crust of the Lhasa terrane to the purely juvenile mantle magmatism underneath the VA-ophiolite (Fig. 8). The collision of the Shyok VA-ophiolite with Eurasia during the Cretaceous Period would have been followed by the reactivation of a new subduction zone along its southern boundary with the northwards dip to initiate the Ladakh Arc, as suggested by Khan *et al.* (1997). This is consistent with the field observations in the Nubra region, where the Late Cretaceous–Eocene Ladakh Batholith intruded into the Shyok Volcanics of the Shyok VA-ophiolite (Fig. 3d, e).

Our geochronological and isotopic data can equally be fitted with a double northwards subduction model (Fig. 9a), and either the Cretaceous or Eocene collision models for the closure of the Shyok Suture. However, issues arise in the case of the latter. There is no documented magmatism within the Karakoram Arc

between 83 and 40 Ma, suggesting that northwards subduction of the Mesotethys beneath Eurasia had ceased by Late Cretaceous time. If the Mesotethys closed after the closure of the Neotethys, as suggested by Bouilhol *et al.*, (2013), then continental-arc magmatism within the Karakoram Arc would be expected to have continued until the final collision during late Eocene time; however, a calc-alkaline magmatism was not recorded within the Karakoram Arc after *c.* 83 Ma (e.g. Groppo *et al.* 2019).

7. Conclusions

The Changmar Complex in the Nubra region of Ladakh formed during Late Jurassic time and has juvenile initial zircon ϵ_{Hf} isotope signatures. It displays geochemical trends characteristic of supra-subduction zone magmatism. The Changmar Complex represents an intrusive suite of a volcanic-arc ophiolite within the Mesotethys Ocean. Upon collision with Eurasia, along the Shyok Suture, this complex formed a basement into which the Cretaceous–Eocene Ladakh Arc has subsequently intruded. Igneous rocks of the Shyok VA-ophiolite in Ladakh show similar field relationships, geochemistry, ages and isotopic characteristics to those from the Jurassic Matum Das tonalite within the Kohistan Arc in Pakistan. We suggest that the Shyok VA-ophiolite and Kohistan Arc were part of the same juvenile, intra-oceanic subduction system, which initiated prior to *c.* 159 Ma. The model presented is consistent with previous models for the amalgamation of Tibet along the Bangong Suture, and it adds a new Jurassic element which allows for correlations to the west. A link between the tectonic developments in the Ladakh and Kohistan regions, and with those in Tibet, maintains the established diachronous E-to-W closure pattern for the Mesotethys Ocean along the Shyok–Bangong Suture.

Supplementary material. To view supplementary material for this article, please visit <https://doi.org/10.1017/S0016756820000400>

Acknowledgments. We thank Jigmet Punchok for field support. Tom McMahon assisted with CL imaging at the UOW Electron Microscopy Centre, Australian Institute for Innovative Materials. José Abrantes and Paul Carr assisted with XRF analysis. We thank Yildirim Dilek and Alastair Robertson for detailed and insightful reviews which helped to improve this manuscript. We also thank Peter Clift, Oliver Jagoutz and Jonathan Aitchison for their constructive comments on earlier versions of this manuscript. Kathryn Goodenough is thanked for editorial handling efforts and helpful comments that helped to improve this manuscript. Rosaria Saktura is thanked for language editing. Funding was provided by the University of Wollongong small grants scheme and supported by an Australian Government Research Training Program Scholarship.

Declaration of interest. None.

References

- Aitchison JC, Ali JR and Davis AM (2007) When and where did India and Asia collide? *Journal of Geophysical Research: Solid Earth* 112(B5), doi: [10.1029/2006JB004706](https://doi.org/10.1029/2006JB004706).
- Aitchison JC, Xia X, Baxter AT and Ali JR (2011) Detrital zircon U–Pb ages along the Yarlung-Tsangpo suture zone, Tibet: implications for oblique convergence and collision between India and Asia. *Gondwana Research* 20, 691–709.
- Allègre CJ, Courtillot V, Tapponnier P, Hirn A, Mattauer M, Coulon C, Jaeger JJ, Achache J, Scharer U, Marcoux J, Burg JP, Girardeau J, Armijo R, Gariépy C, Gopel C, Tindong L, Xuchang X, Chenfa C, Guangqin L, Baoyu L, Jiwen T, Naiwen W, Guoming C, Tonglin H,

- Xibin W, Wanming D, Huaibin S, Yougong C, Ji Z, Hongrong Q, Peisheng B, Songchan W, Bixiang W, Yaoxiu Z and Xu R (1984) Structure and evolution of the Himalaya-Tibet orogenic belt. *Nature* **307**, 17–22.
- Amelin Y, Lee D-C, Halliday AN and Pidgeon RT (1999) Nature of the Earth's earliest crust from hafnium isotopes in single detrital zircons. *Nature* **399**, 252–5.
- Andrews-Speed CP and Brookfield ME (1982) Middle Paleozoic to Cenozoic geology and tectonic evolution of the northwestern Himalaya. *Tectonophysics* **82**, 253–75.
- Bard JP (1983) Metamorphism of an obducted island arc: example of the Kohistan sequence (Pakistan) in the Himalayan collided range. *Earth and Planetary Science Letters* **65**, 133–44.
- Baxter AT, Aitchison J and Zybrev SV (2009) Radiolarian age constraints on Mesotethyan ocean evolution, and their implications for development of the Bangong–Nujiang suture, Tibet. *Journal of the Geological Society* **166**, 689–94.
- Bhutani R, Pande K and Venkatesan TR (2009) 40Ar–39Ar dating of volcanic rocks of the Shyok suture zone in north–west trans-Himalaya: implications for the post-collision evolution of the Shyok suture zone. *Journal of Asian Earth Sciences* **34**, 168–77.
- Bignold SM and Treloar PJ (2003) Northward subduction of the Indian Plate beneath the Kohistan island arc, Pakistan Himalaya: new evidence from isotopic data. *Journal of the Geological Society* **160**, 377.
- Black LP, Kamo SL, Allen CM, Davis DW, Aleinikoff JN, Valley JW, Mundil R, Campbell IH, Korsch RJ, Williams IS and Foudoulis C (2004) Improved 206Pb/238U microprobe geochronology by the monitoring of a trace-element-related matrix effect; SHRIMP, ID–TIMS, ELA–ICP–MS and oxygen isotope documentation for a series of zircon standards. *Chemical Geology* **205**, 115–40.
- Borneman NL, Hodges KV, van Soest MC, Bohon W, Wartho J-A, Cronk SS and Ahmad T (2015) Age and structure of the Shyok suture in the Ladakh region of northwestern India: implications for slip on the Karakoram fault system. *Tectonics* **34**, 2011–33.
- Bouilhol P, Jagoutz O, Hanchar JM and Dudas FO (2013) Dating the India–Eurasia collision through arc magmatic records. *Earth and Planetary Science Letters* **366**, 163–75.
- Bouvier A, Vervoort JD and Patchett PJ (2008) The Lu–Hf and Sm–Nd isotopic composition of CHUR: constraints from unequilibrated chondrites and implications for the bulk composition of terrestrial planets. *Earth and Planetary Science Letters* **273**, 48–57.
- Buckman S, Aitchison JC, Nutman A, Bennett V, Saktura WM, Walsh J, Kachovich S and Hidaka H (2018) The Spongtang Massif in Ladakh, NW Himalaya: an Early Cretaceous record of spontaneous, intra-oceanic subduction initiation in the Neotethys. *Gondwana Research* **63**, 226–49.
- Burg JP (2011) The Asia–Kohistan–India Collision: Review and Discussion. In *Arc-Continent Collision* (eds D Brown and PD Ryan), pp. 279–309. Berlin, Heidelberg: Springer.
- Chapman JB, Scoggin SH, Kapp P, Carrapa B, Ducea MN, Worthington J, Oimahmadov I and Gadoev M (2018) Mesozoic to Cenozoic magmatic history of the Pamir. *Earth and Planetary Science Letters* **482**, 181–92.
- Clift PD, Hannigan R, Blusztajn J and Draut AE (2002) Geochemical evolution of the Dras–Kohistan Arc during collision with Eurasia: evidence from the Ladakh Himalaya, India. *Island Arc* **11**, 255–73.
- Coleman RG (1981) Tectonic setting for ophiolite obduction in Oman. *Journal of Geophysical Research: Solid Earth* **86**, 2497–508.
- Collins AS, Khan MA, Stern RJ, Gribble RF and Windley BF (1998) Discussion on geochemical and isotopic constraints on subduction polarity, magma sources and palaeogeography of the Kohistan Arc, northern Pakistan. *Journal of the Geological Society* **155**, 893–95.
- Cooper LB, Plank T, Arculus RJ, Hauri EH, Hall PS and Parman SW (2010) High-Ca boninites from the active Tonga Arc. *Journal of Geophysical Research: Solid Earth* **115**(B10), doi: [10.1029/2009JB006367](https://doi.org/10.1029/2009JB006367).
- Coward MP, Butler RWH, Khan MA and Knipe RJ (1987) The tectonic history of Kohistan and its implications for Himalayan structure. *Journal of the Geological Society* **144**, 377–91.
- Coward MP, Jan MQ, Rex D, Tarney J, Thirlwall M and Windley BF (1982) Geo-tectonic framework of the Himalaya of N Pakistan. *Journal of the Geological Society* **139**, 299–308.
- Cumming GL and Richards JR (1975) Ore lead isotope ratios in a continuously changing earth. *Earth and Planetary Science Letters* **28**, 155–71.
- Dewey JF (2005) Orogeny can be very short. *Proceedings of the National Academy of Sciences* **102**, 15286–93.
- Dhuime B, Bosch D, Bodinier JL, Garrido CJ, Bruguier O, Hussain SS and Dawood H (2007) Multistage evolution of the Jijal ultramafic–mafic complex (Kohistan, N Pakistan): implications for building the roots of island arcs. *Earth and Planetary Science Letters* **261**, 179–200.
- Dilek Y and Furnes H (2011) Ophiolite genesis and global tectonics: geochemical and tectonic fingerprinting of ancient oceanic lithosphere. *Geological Society of America Bulletin* **123**, 387–411.
- Dilek Y and Furnes H (2019) Tethyan ophiolites and Tethyan seaways. *Journal of the Geological Society* **176**, 899.
- Dilek Y, Furnes H and Shallo M (2008) Geochemistry of the Jurassic Mirdita Ophiolite (Albania) and the MORB to SSZ evolution of a marginal basin oceanic crust. *Lithos* **100**, 174–209.
- Draut AE and Clift PD (2013) Differential preservation in the geologic record of intraoceanic arc sedimentary and tectonic processes. *Earth-Science Reviews* **116**, 57–84.
- Dunlap WJ and Wysoczanski R (2002) Thermal evidence for early Cretaceous metamorphism in the Shyok suture zone and age of the Khardung volcanic rocks, Ladakh, India. *Journal of Asian Earth Sciences* **20**, 481–90.
- Ehiro M, Kojima S, Sato T, Ahmad T and Ohtani T (2007) Discovery of Jurassic ammonoids from the Shyok suture zone to the northeast of Chang La Pass, Ladakh, northwest India and its tectonic significance. *Island Arc* **16**, 124–32.
- Fan J-J, Li C, Xie C-M, Wang M and Chen J-W (2015a) Petrology and U–Pb zircon geochronology of bimodal volcanic rocks from the Maierze Group, northern Tibet: constraints on the timing of closure of the Bangong–Nujiang Ocean. *Lithos* **227**, 148–60.
- Fan JJ, Li C, Xie CM, Wang M and Chen JW (2015b) The evolution of the Bangong–Nujiang Neo-Tethys ocean: evidence from zircon U–Pb and Lu–Hf isotopic analyses of Early Cretaceous oceanic islands and ophiolites. *Tectonophysics* **655**, 27–40.
- Frank W, Gansser A and Trommsdorff V (1977) Geological observations in the Ladakh area (Himalayas), a preliminary report. *Schweizer Mineralogische und Petrographische Mitteilungen* **57**, 89–113.
- Gaetani M (1997) The Karakorum Block in Central Asia, from Ordovician to Cretaceous. *Sedimentary Geology* **109**, 339–59.
- Gaetani M (2016) Blank on the geological map. *Rendiconti Lincei* **27**, 181–95.
- Gansser A (1974) *The Ophiolitic Mélange, a World-wide Problem on Tethyan Examples*. Zürich: Geologisches Institut der Eidgenössischen Technischen Hochschule und der Universität Zürich.
- Gibbons AD, Zahirovic S, Müller RD, Whittaker JM and Yatheesh V (2015) A tectonic model reconciling evidence for the collisions between India, Eurasia and intra-oceanic arcs of the central-eastern Tethys. *Gondwana Research* **28**, 451–92.
- Grosso C, Rolfo F, McClelland WC and Coble MA (2019) Pre-Cenozoic evolution of the Aghil Range (western Tibetan Plateau): a missing piece of the Tibet–Pamir–Karakorum geopuzzle. *Gondwana Research* **69**, 122–43.
- Haider VL, Dunkl I, Eynatten HV, Ding L, Frei D and Zhang L (2013) Cretaceous to Cenozoic evolution of the northern Lhasa Terrane and the Early Paleogene development of peneplains at Nam Co, Tibetan Plateau. *Journal of Asian Earth Sciences* **70–71**, 79–98.
- Hébert R, Bezard R, Guilmette C, Dostal J, Wang CS and Liu ZF (2012) The Indus–Yarlung Zangbo ophiolites from Nanga Parbat to Namche Barwa syntaxes, southern Tibet: first synthesis of petrology, geochemistry, and geochronology with incidences on geodynamic reconstructions of Neo-Tethys. *Gondwana Research* **22**, 377–97.
- Heuberger S, Schaltegger U, Burg J-P, Villa IM, Frank M, Dawood H, Hussain S and Zanchi A (2007) Age and isotopic constraints on magmatism along the Karakoram–Kohistan Suture Zone, NW Pakistan: evidence for subduction and continued convergence after India–Asia collision. *Swiss Journal of Geosciences* **100**, 85–107.

- Hiess J, Bennett VC, Nutman AP and Williams IS (2009) In situ U–Pb, O and Hf isotopic compositions of zircon and olivine from Eoarchaean rocks, West Greenland: new insights to making old crust. *Geochimica et Cosmochimica Acta* **73**, 4489–516.
- Honegger K, Dietrich V, Frank W, Gansser A, Thöni M and Trommsdorff V (1982) Magmatism and metamorphism in the Ladakh Himalayas (the Indus–Tsangpo suture zone). *Earth and Planetary Science Letters* **60**, 253–92.
- Jagoutz O, Bouilhol P, Schaltegger U and Müntener O (2018) The isotopic evolution of the Kohistan Ladakh arc from subduction initiation to continent arc collision. In *Himalayan Tectonics: A Modern Synthesis* (eds PJ Treolar and MP Searle), pp. 165–82. Geological Society, London, Special Publication no. 483.
- Jagoutz O, Royden L, Holt AF and Becker TW (2015) Anomalously fast convergence of India and Eurasia caused by double subduction. *Nature Geoscience* **8**, 475.
- Jan MQ and Asif M (1981) A speculative tectonic model for the evolution of NW Himalaya and Karakoram. *Geological Bulletin of the University of Peshawar* **14**, 199–201.
- Janousek V, Farrow CM and Erban V (2006) Interpretation of whole-rock geochemical data in igneous geochemistry: introducing Geochemical Data Toolkit (GCDkit). *Journal of Petrology* **47**, 1255–59.
- Ji W-Q, Wu F-Y, Chung S-L, Li J-X and Liu C-Z (2009) Zircon U–Pb geochronology and Hf isotopic constraints on petrogenesis of the Gangdese batholith, southern Tibet. *Chemical Geology* **262**, 229–45.
- Juyal KP (2006) Foraminiferal biostratigraphy of the Early Cretaceous Hundiri Formation, lower Shyok area, eastern Karakoram, India. *Current Science* **91**, 1096–101.
- Kapp P and DeCelles PG (2019) Mesozoic–Cenozoic geological evolution of the Himalayan–Tibetan orogen and working tectonic hypotheses. *American Journal of Science* **319**, 159–254.
- Khan MA, Stern RJ, Gribble RF and Windley BF (1997) Geochemical and isotopic constraints on subduction polarity, magma sources, and palaeogeography of the Kohistan intra-oceanic arc, northern Pakistan Himalaya. *Journal of the Geological Society* **154**, 935–46.
- Khan SD, Stern RJ, Mantoni MI, Copeland P, Kimura JI and Khan MA (2004) Age, geochemical and Sr–Nd–Pb isotopic constraints for mantle source characteristics and petrogenesis of Teru Volcanics, Northern Kohistan Terrane, Pakistan. *Tectonophysics* **393**, 263–80.
- Khan SD, Walker DJ, Hall SA, Burke KC, Shah MT and Stockli L (2009) Did the Kohistan–Ladakh island arc collide first with India? *Geological Society of America Bulletin* **121**, 366–84.
- Khan T, Murata M, Karim T, Zafar M, Ozawa H and Hafeez ur R (2007) A Cretaceous dike swarm provides evidence of a spreading axis in the back-arc basin of the Kohistan paleo-island arc, northwestern Himalaya, Pakistan. *Journal of Asian Earth Sciences* **29**, 350–60.
- Kretz R (1983) Symbols for rock-forming minerals. *American Mineralogist* **68**, 277–279.
- Kumar S, Bora S and Sharma UK (2016) Geological appraisal of Ladakh and Tirit granitoids in the Indus–Shyok Suture Zones of northwest Himalaya, India. *Journal of the Geological Society of India* **87**, 737–46.
- Kumar S, Bora S, Sharma UK, Yi K and Kim N (2017) Early Cretaceous subvolcanic calc-alkaline granitoid magmatism in the Nubra–Shyok valley of the Shyok Suture Zone, Ladakh Himalaya, India: evidence from geochemistry and U–Pb SHRIMP zircon geochronology. *Lithos* **277**, 33–50.
- Leier AL, Decelles PG, Kapp P and Ding L (2007) The Takena Formation of the Lhasa terrane, southern Tibet: the record of a Late Cretaceous retroarc foreland basin. *Geological Society of America Bulletin* **119**, 31–48.
- Li G-M, Qin K-Z, Li J-X, Evans NJ, Zhao J-X, Cao M-J and Zhang X-N (2017a) Cretaceous magmatism and metallogeny in the Bangong–Nujiang metallogenic belt, central Tibet: evidence from petrogeochemistry, zircon U–Pb ages, and Hf–O isotopic compositions. *Gondwana Research* **41**, 110–27.
- Li S, Ding L, Guilmette C, Fu J, Xu Q, Yue Y and Henrique-Pinto R (2017b) The subduction-accretion history of the Bangong–Nujiang Ocean: constraints from provenance and geochronology of the Mesozoic strata near Gaize, central Tibet. *Tectonophysics* **702**, 42–60.
- Li S-M, Wang Q, Zhu D-C, Cawood PA, Stern RJ, Weinberg R, Zhao Z and Mo X-X (2020) Reconciling orogenic drivers for the evolution of the Bangong–Nujiang Tethys during Middle–Late Jurassic. *Tectonics*, published online 22 January 2020, e21252, doi: [10.1029/2019TC005951](https://doi.org/10.1029/2019TC005951).
- Li S-M, Zhu D-C, Wang Q, Zhao Z-D, Sui Q-L, Liu S-A, Liu D and Mo X-X (2014) Northward subduction of Bangong–Nujiang Tethys: insight from Late Jurassic intrusive rocks from Bangong Tso in western Tibet. *Lithos* **205**, 284–97.
- Li X-K, Li C, Sun Z-M and Wang M (2017c) Origin and tectonic setting of the giant Duolong Cu–Au deposit, South Qiangtang Terrane, Tibet: evidence from geochronology and geochemistry of Early Cretaceous intrusive rocks. *Ore Geology Reviews* **80**, 61–78.
- Li Y, He J, Wang C, Santosh M, Dai J, Zhang Y, Wei Y and Wang J (2013) Late Cretaceous K-rich magmatism in central Tibet: evidence for early elevation of the Tibetan plateau? *Lithos* **160–161**, 1–13.
- Li Z, Ding L, Lippert PC, Song P, Yue Y and van Hinsbergen DJJ (2016) Paleomagnetic constraints on the Mesozoic drift of the Lhasa terrane (Tibet) from Gondwana to Eurasia. *Geology* **44**, 727–30.
- Liu CZ, Sun-Lin C, Fu-Yuan W, Chang Z, Yang X, Jian-Gang W, Yi C and Shun G (2016) Tethyan suturing in Southeast Asia: Zircon U–Pb and Hf–O isotopic constraints from Myanmar ophiolites. *Geology* **44**, 311–4.
- Liu D, Shi R, Ding L, Huang Q, Zhang X, Yue Y and Zhang L (2017) Zircon U–Pb age and Hf isotopic compositions of Mesozoic granitoids in southern Qiangtang, Tibet: implications for the subduction of the Bangong–Nujiang Tethyan Ocean. *Gondwana Research* **41**, 157–72.
- Liu W-L, Xia B, Zhong Y, Cai J-X, Li J-F, Liu H-F, Cai Z-R and Sun Z-L (2014) Age and composition of the Rebang Co and Julu ophiolites, central Tibet: implications for the evolution of the Bangong Meso-Tethys. *International Geology Review* **56**, 430–47.
- Ludwig K (2008) *Isoplot Version 4.15: A Geochronological Toolkit for Microsoft Excel*. Berkeley: Berkeley Geochronology Center, Special Publication, 247–70.
- Matsumaru K, Ehiro M and Kojima S (2006) On Orbitolina (Foraminiferida) from the Shyok suture zone, Ladakh, NW India. *Journal of the Palaeontological Society of India* **51**, 43–49.
- Metcalfe I (1996) Pre-Cretaceous evolution of SE Asian terranes. In *Tectonic Evolution of Southeast Asia* (eds R Hall and D Blundell), pp. 97–122. Geological Society, London, Special Publication no. 106.
- Metcalfe I (2013) Gondwana dispersion and Asian accretion: tectonic and palaeogeographic evolution of eastern Tethys. *Journal of Asian Earth Sciences* **66**, 1–33.
- Pearce JA (1982) Trace element characteristics of lavas from destructive plate boundaries. In *Andesites: Orogenic Andesites and Related Rocks* (ed. RS Thorpe), pp. 525–48. Chichester, England: John Wiley and Sons.
- Pearce JA (2008) Geochemical fingerprinting of oceanic basalts with applications to ophiolite classification and the search for Archean oceanic crust. *Lithos* **100**, 14–48.
- Pedersen RB, Searle MP and Corfield RI (2001) U–Pb zircon ages from the Spontang Ophiolite, Ladakh Himalaya. *Journal of the Geological Society* **158**, 513–20.
- Petterson MG and Treloar PJ (2004) Volcanostratigraphy of arc volcanic sequences in the Kohistan arc, North Pakistan: volcanism within island arc, back-arc-basin, and intra-continental tectonic settings. *Journal of Volcanology and Geothermal Research* **130**, 147–78.
- Petterson MG and Windley BF (1985) Rb–Sr dating of the Kohistan arc-batholith in the Trans-Himalaya of north Pakistan, and tectonic implications. *Earth and Planetary Science Letters* **74**, 45–57.
- Petterson MG and Windley BF (1991) Changing source regions of magmas and crustal growth in the Trans-Himalayas: evidence from the Chalt volcanics and Kohistan batholith, Kohistan, northern Pakistan. *Earth and Planetary Science Letters* **102**, 326–41.
- Phillips RJ (2008) Geological map of the Karakoram fault zone, eastern Karakoram, Ladakh, NW Himalaya. *Journal of Maps* **4**(1), 21–37.
- Phillips RJ, Parrish RR and Searle MP (2004) Age constraints on ductile deformation and long-term slip rates along the Karakoram fault zone, Ladakh. *Earth and Planetary Science Letters* **226**, 305–19.
- Pudsey CJ (1986) The Northern Suture, Pakistan: margin of a Cretaceous island arc. *Geological Magazine* **123**, 405–23.

- Pullen A, Kapp P, Gehrels GE, Ding L and Zhang Q (2011) Metamorphic rocks in central Tibet: lateral variations and implications for crustal structure. *GSA Bulletin* **123**, 585–600.
- Pundir S, Adlakha V, Kumar S and Singhal S (2020) Closure of India–Asia collision margin along the Shyok Suture Zone in the eastern Karakoram: new geochemical and zircon U–Pb geochronological observations. *Geological Magazine*, published online 24 February 2020, doi: [10.1017/S0016756819001547](https://doi.org/10.1017/S0016756819001547).
- Rai H (1983) Geology of the Nubra Valley and its significance on the evolution of the Ladakh Himalaya. In *Geology of Indus Suture Zone of Ladakh* (eds VC Thakur and KK Sharma), pp. 79–97. Dehradun, India: Wadia Institute of Himalayan Geology.
- Ravikant V, Wu F-Y and Ji W-Q (2009) Zircon U–Pb and Hf isotopic constraints on petrogenesis of the Cretaceous–Tertiary granites in eastern Karakoram and Ladakh, India. *Lithos* **110**, 153–66.
- Reagan MK, Pearce JA, Petronotis K, Almeev RR, Avery AJ, Carvalho C, Chapman T, Christeson GL, Ferré EC, Godard M, Heaton DE, Kirchenbaur M, Kurz W, Kutterolf S, Li H, Li Y, Michibayashi K, Morgan S, Nelson WR, Prytulak J, Python M, Robertson AHF, Ryan JG, Sager WW, Sakuyama T, Shervais JW, Shimizu K and Whattam SA (2017) Subduction initiation and ophiolite crust: new insights from IODP drilling. *International Geology Review* **59**, 1439–50.
- Reuber I (1990) Les ophiolites de la Shyok dans l'Himalaya du Ladakh: reliques de la plaque océanique de la Tethys surmontée d'un arc volcanosédimentaire daté du Crétacé moyen. *Comptes rendus de l'Académie des sciences. Série 2, Mécanique, Physique, Chimie, Sciences de l'univers, Sciences de la Terre* **310**, 1255–62 (in French with English abstract).
- Rex AJ, Searle MP, Tirrul R, Crawford MB, Prior DJ, Rex DC and Barnicoat A (1988) The geochemical and tectonic evolution of the central Karakoram, North Pakistan. *Philosophical Transactions of the Royal Society of London. Series A, Mathematical and Physical Sciences* **326**, 229–55.
- Robertson A and Degnan P (1994) The Dras arc Complex: lithofacies and reconstruction of a Late Cretaceous oceanic volcanic arc in the Indus Suture Zone, Ladakh Himalaya. *Sedimentary Geology* **92**, 117–45.
- Robertson AHF and Collins AS (2002) Shyok Suture Zone, N Pakistan: late Mesozoic–Tertiary evolution of a critical suture separating the oceanic Ladakh Arc from the Asian continental margin. *Journal of Asian Earth Sciences* **20**, 309–51.
- Robinson AC (2009) Geologic offsets across the northern Karakoram fault: implications for its role and terrane correlations in the western Himalayan–Tibetan orogen. *Earth and Planetary Science Letters* **279**, 123–30.
- Rolland Y, Pêcher A and Picard C (2000) Middle Cretaceous back-arc formation and arc evolution along the Asian margin: the Shyok Suture Zone in northern Ladakh (NW Himalaya). *Tectonophysics* **325**, 145–73.
- Ryan WB, Carbotte SM, Coplan JO, O'Hara S, Melkonian A, Arko R, Weissel RA, Ferrini V, Goodwillie A, Nitsche F and Bonczkowski J (2009) Global multi-resolution topography synthesis. *Geochemistry, Geophysics, Geosystems*, **10**(3), doi: [10.1029/2008GC002332](https://doi.org/10.1029/2008GC002332).
- Schaltegger U, Frank M and Burg JP (2003) A 120 million years record of magmatism and crustal melting in the Kohistan Batholith. In *Proceedings of EGS-AGU-EUG Joint Assembly*, 6–11 April 2003, Nice, France.
- Schaltegger U, Zeilinger G, Frank M and Burg JP (2002) Multiple mantle sources during island arc magmatism: U–Pb and Hf isotopic evidence from the Kohistan arc complex, Pakistan. *Terra Nova* **14**, 461–68.
- Schärer U, Hamet J and Allègre CJ (1984) The Transhimalaya (Gangdese) plutonism in the Ladakh region: a U–Pb and Rb–Sr study. *Earth and Planetary Science Letters* **67**, 327–39.
- Searle M and Cox J (1999) Tectonic setting, origin, and obduction of the Oman ophiolite. *Geological Society of America Bulletin* **111**, 104–22.
- Searle MP, Cooper DJW and Rex AJ (1988) Collision tectonics of the Ladakh–Zaskar Himalaya. *Philosophical Transactions of the Royal Society of London. Series A, Mathematical and Physical Sciences* **326**, 117–50.
- Searle MP and Hacker BR (2018) Structural and metamorphic evolution of the Karakoram and Pamir following India–Kohistan–Asia collision. In *Himalayan Tectonics: A Modern Synthesis* (eds PJ Treolar and MP Searle), pp. 555–82. Geological Society, London, Special Publication no. 483.
- Searle MP, Khan MA, Fraser JE, Gough SJ and Jan MQ (1999) The tectonic evolution of the Kohistan–Karakoram collision belt along the Karakoram Highway transect, north Pakistan. *Tectonics* **18**, 929–49.
- Searle MP, Parrish RR, Tirrul R and Rex DC (1990) Age of crystallization and cooling of the K2 gneiss in the Baltoro Karakoram. *Journal of the Geological Society* **147**, 603–06.
- Searle MP and Treolar PJ (2019) An introduction to Himalayan tectonics: a modern synthesis. In *Himalayan Tectonics: A Modern Synthesis* (eds PJ Treolar and MP Searle), pp. 1–17. Geological Society, London, Special Publication no. 483.
- Searle MP, Windley BF, Coward MP, Cooper DJW, Rex AJ, Rex D, Tingdong LI, Xuchang X, Jan MQ, Thakur VC and Kumar S (1987) The closing of Tethys and the tectonics of the Himalaya. *GSA Bulletin* **98**, 678–701.
- Sen K and Collins AS (2013) Dextral transpression and late Eocene magmatism in the trans-Himalayan Ladakh Batholith (North India): implications for tectono-magmatic evolution of the Indo-Eurasian collisional arc. *International Journal of Earth Sciences* **102**, 1895–909.
- Şengör AMC (1984) Introduction: the history of the Tethys concept. In *The Cimmeride Orogenic System and the Tectonics of Eurasia* (ed AMC Şengör), pp. 1–82. Boulder: Geological Society of America.
- Seton M, Müller RD, Zahirovic S, Gaina C, Torsvik T, Shephard G, Talsma A, Gurnis M, Turner M, Maus S and Chandler M (2012) Global continental and ocean basin reconstructions since 200Ma. *Earth-Science Reviews* **113**, 212–70.
- Sharma KK, Sinha AK, Bagdasarian GP and Gukasian RC (1978) Potassium argon dating of Dras volcanics, Shyok volcanics and Ladakh granite, Ladakh, northwest Himalaya. *Himalayan Geology* **8**, 288–95.
- Shervais JW (1982) Ti–V plots and the petrogenesis of modern and ophiolite lavas. *Earth and Planetary Science Letters* **59**, 101–18.
- Singh S, Kumar R, Barley ME and Jain AK (2007) SHRIMP U–Pb ages and depth of emplacement of Ladakh Batholith, Eastern Ladakh, India. *Journal of Asian Earth Sciences* **30**, 490–503.
- Sláma J, Košler J, Condon DJ, Crowley JL, Gerdes A, Hanchar JM, Horstwood MSA, Morris GA, Nasdala L, Norberg N, Schaltegger U, Schoene B, Tubrett MN and Whitehouse MJ (2008) Plešovice zircon — A new natural reference material for U–Pb and Hf isotopic microanalysis. *Chemical Geology* **249**, 1–35.
- Soesoo A, Bons PD, Gray DR and Foster DA (1997) Divergent double subduction: tectonic and petrologic consequences. *Geology* **25**, 755–58.
- Stern RA, Bodorkos S, Kamo SL, Hickman AH and Corfu F (2009) Measurement of SIMS instrumental mass fractionation of Pb isotopes during zircon dating. *Geostandards and Geoanalytical Research* **33**, 145–68.
- Stern RJ, Reagan M, Ishizuka O, Ohara Y and Whattam S (2012) To understand subduction initiation, study forearc crust: to understand forearc crust, study ophiolites. *Lithosphere* **4**, 469–83.
- St-Onge MR, Rayner N and Searle MP (2010) Zircon age determinations for the Ladakh batholith at Chumathang (Northwest India): implications for the age of the India–Asia collision in the Ladakh Himalaya. *Tectonophysics* **495**, 171–83.
- Sun SS and McDonough WF (1989) Chemical and isotopic systematics of oceanic basalts: implications for mantle composition and processes. *Geological Society, London, Special Publications* **42**, 313–45.
- Tahirkheli RAK, Mattauer M, Proust F and Tapponnier P (1979) The India Eurasia Suture Zone in northern Pakistan: synthesis and interpretation of recent data at plate scale. In *Geodynamics of Pakistan* (eds A Farah and KA De Jong), pp. 125–30. Quetta: Geological Survey of Pakistan.
- Thakur VC, Viridi NS, Rai H and Gupta KR (1981) A note on the geology of Nubra-Shyok area of Ladakh, Kashmir, Himalaya. *Geological Society of India* **22**, 46–50.
- Thanh NX, Itaya T, Ahmad T, Kojima S, Ohtani T and Ehiro M (2010) Mineral chemistry and K–Ar ages of plutons across the Karakoram fault in the Shyok–Nubra confluence of northern Ladakh Himalaya, India. *Gondwana Research* **17**, 180–88.
- Thanh NX, Rajesh VJ, Itaya T, Windley B, Kwon S and Park C-S (2012) A Cretaceous forearc ophiolite in the Shyok suture zone, Ladakh, NW India: implications for the tectonic evolution of the Northwest Himalaya. *Lithos* **155**, 81–93.

- Treloar PJ, Petterson MG, Jan MQ and Sullivan MA** (1996) A re-evaluation of the stratigraphy and evolution of the Kohistan arc sequence, Pakistan Himalaya: implications for magmatic and tectonic arc-building processes. *Journal of the Geological Society* **153**, 681–93.
- Treloar PJ, Rex DC, Guise PG, Coward MP, Searle MP, Windley BF, Petterson MG, Jan MQ and Luff IW** (1989) K-Ar and Ar-Ar geochronology of the Himalayan collision in NW Pakistan: constraints on the timing of suturing, deformation, metamorphism and uplift. *Tectonics* **8**, 881–909.
- Trivedi JR, Gopalan K, Kisharma K, Gupta KR and Choubey VM** (1982) Rb–Sr age of Gaik granite, Ladakh batholith, northwest Himalaya. *Proceedings of the Indian Academy of Sciences - Earth and Planetary Sciences* **91**, 65–73.
- Upadhyay R** (2001) Middle Cretaceous carbonate build-ups and volcanic seamount in the Shyok suture, northern Ladakh, India. *Current Science* **81**, 695–99.
- Upadhyay R** (2014) Palaeogeographic significance of “Yasin-type” rudist and orbitolinid fauna of the Shyok Suture Zone, Saltoro Hills, northern Ladakh, India. *Current Science* **106**, 223–8.
- Upadhyay R, Frisch W and Siebel W** (2008) Tectonic implications of new U–Pb zircon ages of the Ladakh batholith, Indus suture zone, northwest Himalaya, India. *Terra Nova* **20**, 309–17.
- Upadhyay R, Sinha AK, Chandra R and Rai H** (1999) Tectonic and magmatic evolution of the eastern Karakoram, India. *Geodinamica Acta* **12**, 341–58.
- Walsh JMJ, Buckman S, Nutman AP and Zhou R** (2019) Age and provenance of the Nindam Formation, Ladakh, NW Himalaya: evolution of the Intraoceanic Dras Arc before collision with India. *Tectonics* **38**, 3070–96.
- Wang LQ, Pan GT, Ding J and Yao DS** (2013) *Guidebook of 1:1,500,000 Geological Map of the Qinghai–Xizang (Tibet) Plateau and Adjacent Areas*. Beijing, China: Geological Publishing House.
- Ward CD, McArthur JM and Walsh JN** (1992) Rare earth element behaviour during evolution and alteration of the Dartmoor Granite, SW England. *Journal of Petrology* **33**, 785–815.
- Weinberg RF and Dunlap WJ** (2000) Growth and deformation of the Ladakh Batholith, Northwest Himalayas: implications for timing of continental collision and origin of calc-alkaline batholiths. *The Journal of Geology* **108**, 303–20.
- Weinberg RF, Dunlap WJ and Whitehouse M** (1999) New field, structural and geochronological data from the Shyok and Nubra valleys, northern Ladakh: linking Kohistan to Tibet. In *Tectonics of the Nanga Parbat Syntaxis and the Western Himalaya* (eds MA Khan, PJ Treloar, MP Searle and MQ Jan), pp. 253–75. Geological Society, London, Special Publication no. 170.
- White LT, Ahmad T, Ireland TR, Lister GS and Forster MA** (2011) Deconvolving episodic age spectra from zircons of the Ladakh Batholith, northwest Indian Himalaya. *Chemical Geology* **289**, 179–96.
- Williams IS** (1998) U–Th–Pb geochronology by ion microprobe. *Reviews in Economic Geology* **7**, 1–35.
- Woodhead JD and Hergt JM** (2005) A preliminary appraisal of seven natural zircon reference materials for in situ Hf isotope determination. *Geostandards and Geoanalytical Research* **29**, 183–95.
- Yan M, Zhang D, Fang X, Ren H, Zhang W, Zan J, Song C and Zhang T** (2016) Paleomagnetic data bearing on the Mesozoic deformation of the Qiangtang Block: implications for the evolution of the Paleo- and Meso-Tethys. *Gondwana Research* **39**, 292–316.
- Yin A and Harrison TM** (2000) Geologic evolution of the Himalayan–Tibetan Orogen. *Annual Review of Earth and Planetary Sciences* **28**, 211–80.
- Zanchetta S, Worthington J, Angiolini L, Leven EJ, Villa IM and Zanchi A** (2018) The Bashgumbaz Complex (Tajikistan): arc obduction in the Cimmerian orogeny of the Pamir. *Gondwana Research* **57**, 170–90.
- Zhou S, Mo X, Dong G, Zhao Z, Qiu R, Guo T and Wang L** (2004) ⁴⁰Ar–³⁹Ar geochronology of Cenozoic Linzizong volcanic rocks from Linzhou Basin, Tibet, China, and their geological implications. *Chinese Science Bulletin* **49**, 1970–79.
- Zhu D-C, Li S-M, Cawood PA, Wang Q, Zhao Z-D, Liu S-A and Wang L-Q** (2016) Assembly of the Lhasa and Qiangtang terranes in central Tibet by divergent double subduction. *Lithos* **245**, 7–17.
- Zhu D-C, Zhao Z-D, Niu Y, Dilek Y, Hou Z-Q and Mo X-X** (2013) The origin and pre-Cenozoic evolution of the Tibetan Plateau. *Gondwana Research* **23**, 1429–54.
- Zhu D-C, Zhao Z-D, Niu Y, Mo X-X, Chung S-L, Hou Z-Q, Wang L-Q and Wu F-Y** (2011) The Lhasa Terrane: record of a microcontinent and its histories of drift and growth. *Earth and Planetary Science Letters* **301**, 241–55.